RADIOACTIVITY AND ELEMENTAL ANALYSIS OF CARBONATITE ROCKS FROM PARTS OF GWASI AREA, SOUTH WESTERN KENYA

By

Achola Shem Opiyo

I56/7426/2004

A thesis submitted in partial fulfillment for the requirements for the award of degree of Master of Science (physics) of University of Nairobi
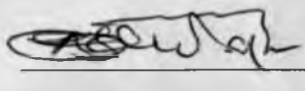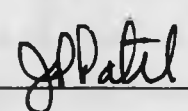
2009

DECLARATION

This thesis is my original work and has not been presented for a degree by any other University
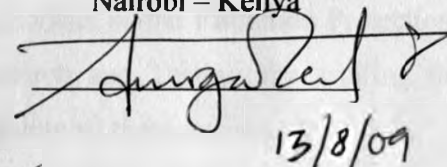
(signature) . 12/8/09

Achola Shem Opiyo
Department of Physics
University of Nairobi
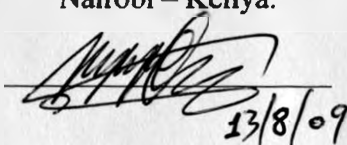
This thesis has been submitted for examination with the approval of my University supervisors:

1.   _(signature)_ 12/8/09

Prof. J. P. Patel
Department of Physics
University of Nairobi
Nairobi – Kenya

2.   _(signature)_
13/8/09

Dr. A. O. Mustapha
Department of Physics
University of Nairobi
Nairobi – Kenya.

3.   _(signature)_
13/8/09

Mr. D. M. Maina
Institute of Nuclear Science and Technology
University of Nairobi
Nairobi – Kenya.

ACKNOWLEDGEMENTS

TABLE OF CONTENTS

LIST OF FIGURES.

LIST OF TABLES.

LIST OF ABBREVIATIONS, SYMBOLS AND ACRONYMS

UNSCEAR: United Nations Scientific Committee on the Effects of Atomic Radiation.

IAEA: International Atomic Energy Agency.

ICRP: International Commission on Radiological Protection.

HBRA: High Background Radiation Area.

AQCS: Analytical Quality Control Services.

CA: Control Area.

EDXRF: Energy Dispersive X-Ray Fluorescence.

XRF: X-Ray Fluorescence.

NCRP: National Council on Radiation Protection and Measurements.

Abstract

Rocks and soils from a number of areas underlied by carbonatite rocks in Kenya have been associated with high radioactivity. In this thesis, the analyzed results of the background radiation measurements in the field, activity concentrations of primordial radionuclides in the samples, approximated annual external effective dose rates and the elemental concentrations of samples from Ruri hills have been presented. Ruri hills are roughly between latitudes 0°30'S and 1°00'S, bounded on the east by longitude 34°30'E and on the west by the shores of Lake Victoria and the Winnam Gulf. Altitudes range from about 1000m on the shores of Lake Victoria to above 1800m on top of the Ruri hills. Gamma spectrometric analyses of twenty one samples from South and North Ruri hills in Lambwe east location of Suba District, south western Kenya, have been carried out using high-purity germanium (HPGe) gamma-ray detector. The samples comprise rocks (mainly carbonatite) and soils. The activity concentrations ranged from 14.18 to 6559.99 Bq kg^{-1} with an average of 1396.85 Bq kg^{-1} for thorium-232, from 2.73 to 499.24 Bq kg^{-1} with an average of 178.69 Bq kg^{-1} for uranium-238 equivalent, and from 56.67 to 1454.73 Bq kg^{-1} with an average of 508.67 Bq kg^{-1} for potassium-40. The corresponding ranges of elemental concentrations, and the mean values in μg g^{-1} are 25.15-1346.67, 280.04; 6.89-137.33, 27.91; and 438.00-3060.00, 1345.90; for thorium, uranium and potassium respectively. Other elements identified in the samples are: Ca, Ti, Mn, Fe, Zn, Au, Pb, Rb, Sr, Y, Ce, Zr, Nb, and Mo. Their concentrations are shown in tables 5.5 and 5.6. Absorbed dose rates in air outdoors at approximately 1m above the ground were measured using survey meters. The values are in the range of 700 to 6000.00 nG yh^{-1}, with an overall mean value of 2325.84 nGy h^{-1}. These values correspond to individual annual effective dose rates ranging from 1.717 to 14.717 mSv yr^{-1} with an overall mean of 5.705 mSv yr^{-1}, assuming a 40% (0.4) occupancy factor. Thus, annual external effective dose rates at Ruri hills are much higher than the global average of 0.46 mSv yr^{-1} (i.e. approximately twelve times the global average).

Chapter 1

INTRODUCTION

High levels of natural background radiation have been reported in many areas of the world for example in Guangdong province China [Wei et al., 1993], South west coast of India [Sunta, 1993], Ramsar area in the Republic of Iran [Sohrabi, 1995], Punjab Province of Pakistan [Tahir et al. 2005], and Mrima hills of South coast Kenya [Patel, 1991]. These high levels of background radiation are due to the occurrence of anomalous concentrations of the naturally occurring radionuclides in the environment, (rock, soil, water etc). This is the so called terrestrial natural sources of radiation.

In the case of Mrima hills, the high background radiation is attributed to the presence of weathered carbonatite rock with high concentration of thorium. Patel (1991) showed that radiation absorbed dose rate in air ranged from 200 nGy h^{-1} to 14000 nGy h^{-1}, which is extremely high compared to 60 nGy h^{-1} which is the global population weighted average value [UNSCEAR, 2000].

The other natural components of background radiation include cosmic rays and radiation from cosmogenic radionuclides. Cosmic radiation refers to both the primary energetic radiation from solar and galactic events. When the primary radiation showers the earth's atmosphere, they undergo reactions and transform to secondary radiation. The cosmic radiation at the lower atmosphere (0 to 3km) consists almost entirely of secondary component. Annual external dose rates from cosmic rays depend partly on latitude and altitude of the place. The latitude effect is due to the charged particle nature of the primary cosmic rays. When they come near the earth, its magnetic field tends to deflect the rays away from the equator and lower latitudes, and the deflection reduces toward the poles [UNSCEAR, 2000; Rasolonjatovo et al., 2002]. For example, the average external dose from cosmic radiation is 305 μSv yr^{-1} at lower latitudes (<30°) and greater than 350 μSv yr^{-1} at higher latitudes (50° and above). The average values also increase with altitude; from 340 μSv yr^{-1} at sea levels to 460 μSv yr^{-1} at 1000 m. [UNSCEAR, 2000; Rasolonjatovo et al., 2002].

The area investigated in the present study is Ruri hills, formerly known as Gwasi, in Suba district of South Western Kenya. It is bordered by latitudes 0˚30'S, 1˚00'S and longitude 34˚30'E and by the shores of Lake Victoria. The altitudes of the area vary from 1000 m at the shores of Lake Victoria to about 1850 m at the highest points. The people living in these areas are mostly peasant farmers, i.e. they practice both small scale crop and animal farming. Sources of water are boreholes, dams, seasonal rivers and Lake Victoria.

Outcrops of carbonatite rocks are found in the various locations including the Ruri hills complex, Rangwa ring complex, Kuge and Soklo point. While doing geological mapping of Gwasi area McCall (1958) reported radioactivity of between 5 to 10 times the natural background radiations; ten times at Ruri hills, ten times at Kuge and two times at Soklo point. A similar radiation pattern was reported at the Rangwa ring complex.

Such high levels of natural background radiations have been associated with minerals such as monazites and pyrochlore, which can be of economic value [Karam, 2002]. Hence this is an important reason to investigate the elemental composition of the carbonatite rocks in these areas. Also, from the point of view of the health of the inhabitants of these areas; it is noted that the oxides of some of the radioactive nuclides are soluble and could go into the food chain.

The study involved field works during which the absorbed dose in air at about 1m above ground was measured using Berthold Y-Analyzer LB-125 survey meter as the areas were traversed on foot. The inhabited sections of the hills were given priorities, this include homesteads, farmlands, school areas etc. Samples of soil, rocks and water points were also taken and analyzed later in the laboratory using x-ray fluorescence and gamma-ray analyses.

The elemental analysis of the samples give indications of the mineral prospects of the areas under study while the activity concentration of the naturally occurring radionuclides and the estimated and measured doses also give some indication about the radiological consequence of the natural sources [Tiwari et al., 2001; Mohammadi et al., 2006].

1.1 STATEMENT OF THE RESEARCH PROBLEM

The health effects of chronic exposure to low background levels of radiation are poorly understood and there is need for further studies in this area. Such studies are not easily carried out in the laboratory settings because they require large populations of the subjects, e.g. human, animals, etc. The high background radiation areas, however, present unique opportunities for these studies. Results of studies so far carried out in some parts of the world's high background radiation areas (e.g. Guangdong and Yangjiang provinces in China, Kerala and Madras in India, Ramsar in Iran etc) are generally inconclusive and sometimes contradictory. Kenya also has a number of high background radiation areas (e.g. Mrima hill, Ruri hills, Rangwa complex, Koru etc) but no such research is being carried out. The present study is therefore proposed to exploit the rare opportunity presented by the presence of these high background radiation areas in Kenya to study this phenomenon.

1.2 HYPOTHESIS

Residents of Gwasi area are exposed to high background radiation levels as reported by McCall (1958). There is need therefore to investigate radiation levels in this region and its environs.

1.3 OBJECTIVES OF THE RESEARCH PROJECT

1.3.1 GENERAL OBJECTIVE

To determine environmental radioactivity level and elemental concentrations of rock and soil samples from Gwasi area in Suba district (e.g Ruri Hills).

1.3.2 Specific objectives;

(i) To measure the absorbed gamma dose rates in air above soil containing uniform distribution of radio- nuclides (^{232}Th, ^{238}U and ^{40}K) using Gamma-ray survey meter.

(ii) To determine radionuclide content (i.e. activity concentrations) of rock samples from Ruri hills.

3

(iii) To estimate the annual external effective dose rates from the activity concentrations.

(iv) To determine the elemental concentrations in rock samples from Ruri hills using Energy dispersive x-ray fluorescence (EDXRF) method.

1.4 RELEVANCE OF THE RESEARCH PROJECT

Radiation absorbed dose in high background radiation areas can be several times the values in the normal natural background radiation areas. Using rocks and soils from these areas for construction of roads, houses, e.t.c., may result in an unacceptable external exposure due to gamma-ray radiation emitted from the materials (rocks, soil) [Patel, 1991]. It is yet to be determined if this could result in health hazards for the inhabitants of these areas, although radioecological surveys carried out in some other high background radiation areas [Sohrabi, 1995; Wei, 1993; NCPR Report, 1987] have shown some adverse health effects such as Down's Syndrome, mental retardation, physical deformity, etc. This research will therefore provide useful information on the levels of radiation dose in some of the HBRA's in Kenya.

Also from the economic point of view, carbonatite rocks are known to associate with rare-earth elements (REE) minerals. Thus, the elemental analysis of the samples from these areas should determine the presence of these elements and their quantities. In this regard the proposed study will serve as a mineral prospecting survey.

4

Chapter 2

LITERATURE REVIEW

2.1 HIGH BACKGROUND RADIATION AREAS (HBRAs)

The existence of high-level natural radiation areas is attributed to the availability of certain radioactive minerals or elements embedded in the continental rock system of these areas. Carbonatites containing monazite and ironstones are major sources of radioactivity due to high concentrations of thorium and uranium together with their radioactive daughters [McCall, 1958; Karam, 2002].

High-level background radiation areas have unique characteristics, which provide rare opportunities for studying the behaviour of radionuclides in the environment. These areas are natural laboratories for researchers on the behaviour of radionuclides in the environment and on the effect of low level radiation dose and dose rate [Karam, 2002; Kauffman, 2003]. Over the years radioecological studies have been carried out in high background radiation areas of the world and the findings of studies on the health effects of low levels of radiation are still inconclusive (Mohammadi et al., 2006). A survey by Sohrabi (1995) in the high level natural radiation area of Ramsar in Iran indicated that measured environmental gamma exposures vary between 70 to 1.7×10^4 nGy h^{-1} for outdoor and indoor exposures; the potential exposure in houses range from 0.6 to 360 mGy yr^{-1} as measured by thermo-luminescence dosimeters (TLDs), film badges and survey meters and radon levels measured from 20 to 3.7×10^5 Bq m^{-3} with corresponding effective doses up to 98.3 mSv yr^{-1} in drinking water and hot springs. Sohrabi concluded that the high level radioactivity seemed to be due to the sulfurous mineral waters having a fomeroline origin in a volcanic activity which finally found their way to the surface due to geological processes. The radioactivity in the water samples was due to the mineral water springs passing through the streams leaving radioactivity residues filtered by the soil and also due to some travertine deposits having thorium content more than that of uranium [Karam, 2002].

A similar health survey [Wei, 1980] was carried out in the high background radiation area (HBRA) in Yangjiang of Guangdong province (China) and the neighbouring area which was designated as a control area (CA). The investigated high-level background radiation areas covered a total area of about 500 square kilometers. The sources of background radiation were nearby mountains whose surface rocks were found to be granites from which fine particles of monazite were washed down continuously year by year by rain and deposited in the surrounding basin region resulting in the elevation of the levels of the background radiation. The results of the analyses of soil samples by spectrometry and radiochemistry [Tahir et al., 2005] as well as the measurements of field gamma spectrometry showed that the concentrations of natural radionuclides in soil were quite different between the two areas designated as HBRA and control area (CA), especially that of thorium which was about six times higher in high level natural background radiation area than that in control area.

Very high background radiation levels have also been found at Guarapari, [Freital et al.,] coastal region of Esperito Santo and the Morro Do Forro in Minas Gerais [Ajlouni et al., 2009] in Brazil; Yangjiang in China [Wei et al., 1993]; southwest coast of India [Sunta, 1993; Selvasekarapandian et al., 1999]; Ramsar in Iran [Sorahbi, 1995; Karam,2002]; in parts of the United States and Canada [NCRP, 1987], and in some other countries [UNSCEAR, 2000; Morishima et al. 2000].

Examples of high background radiation areas in Kenya are Mrima hill [Mangala, 1987; Patel, 1991; Mustapha, 1999]; Ruri hills, Rangwa ring complex, Soklo point and Kuge (Tuige), in Gwasi, Suba district [McCall, 1958]. In particular, Mangala (1987) conducted elemental analysis of soil and rock samples from Mrima hills in which thorium and traces of rare earth metals were found in high concentrations (>1000 µg/g). Patel (1991), in later studies determined that the Mrima area is composed of deeply weathered carbonatite rock and has high natural radioactivity. In the same study, Patel detected that the road built using rocks and soil from Mrima hill posed health hazard to road users.

His work to study the radiation distribution pattern showed that boreholes in the area may contain high radiation anomalies while the external radiation in the Mrima hill ambient

6

atmosphere was found to be fifty three times higher than the natural background effective dose rate (200 nGy h^{-1} to 1.4×10^4 nGy h^{-1}) which is much higher than the global annual effective dose rate. Patel reported that the geological structure of the area is masked by deep soil and weathered rock that cover up to 180 metres in thickness in some places. The residual deposit weathered rocks amount to 7.77×10^6 metric tones [Patel, 1991]. Mustapha (1999) tested water samples from boreholes in the same vicinity and determined anomalous levels of radon in drinking water samples [Mustapha et al, 2002].

2.2 GEOLOGICAL FACTORS RESPONSIBLE FOR THE ENRICHMENT OF HEAVY MINERALS

Radiogenic analysis of various fractions of heavy mineral sands from Erasama beach in India shows that monazite and zircon sands are highly radioactive [Mohanty et al., 2004]. Monazite is a natural phosphate mineral one of the principal sources of rare earth elements (REE'S) and thorium in the continental crust. The actinide incorporation into monazite crystal lattices is dominated by thorium, as compared to uranium as observed in all monazite samples, especially those of granitic origin. The abundance of thorium typically about 10 % (by weight) and that of uranium about 0.5 % (by weight) are found in monazite crystals [Mohanty et al., 2004]. On the other hand, zircon contains 5-4000 µg/g of uranium and 2-2000 µg/g of thorium [Deer et al., 1995].

Shear zones are regions of high radon concentrations, especially in mountain belts. Shear zones developed in rocks having uranium concentration, such as granitic rocks have a high probability of causing an indoor problem. It has been shown that high radon levels in water accompany high soil radon [Edsfeldt, 2001]. Preliminary water data from shear zones, the Hylas fault in Virginia and a brittle shear fault in the silver plume Quartz monazite near Canifer, indicate that many domestic wells have radon concentrations greater than 3.7×10^5 Bq/m^3 [Edsfedt, 2001] . High radon emanation, especially along fracture surfaces, contributes to radon concentration in water. In areas with elevated naturally occurring radioactive materials, the type of soil, building materials, and water used for drinking and other household uses can make variable contributions to the indoor radon-222 level.

McCall (1958) analyzed radioactive ironstone from Gwasi area but found no obvious radioactive mineral. He put magnetite at approximately 35% and calcium at 23% as major constituents. However, he tentatively identified monazite and pyrochlore: monazite contains principally thorium and its radioactive daughters along with several rare earth metals. The high radioactivity up to 15 times the background is however, too great to be accounted for by monazite and pyrochlore alone. Thus, it is suspected that other radioactive minerals are present in the iron stone ores. With these in mind, it is necessary to investigate the activity concentration of radioactive elements and the associated radiation dose levels around the Ruri hills.

Monazite had been identified in the soil samples from Suba district [McCall, 1958]. Pyrochlore was detected in two specimens from North Ruri and also present in the carbonatites of the nearby vent of Kuge [Bear, 1952; Idman, 1984]. Again the high radioactivity observed (up to 15 times the background) was, however, too high to be accounted for by monazite and pyrochlore alone especially in view of their sparse distribution. This in essence means that some other radioactive materials beside thorium are probably present in the iron ores within the area [Akhtar et al., 2005].

2.3 TERRESTRIAL AND COSMOGENIC RADIONUCLIDES

Natural radioactivity arises from cosmogenic and primordial radionuclides. Cosmogenic radionuclides such as ^3H, ^7Be, ^{14}C and ^{22}Na, are produced by the interaction of cosmic-rays (mainly high–energetic protons) with elements in the earth's atmosphere [UNSCEAR, 2000]. The most important cosmogenic radionuclide produced is carbon-14. Once produced, it is oxidized to carbon dioxide. Most of the other cosmogenically produced radionuclides in the atmosphere are oxidized and become attached to aerosol particles, which act as condensation nuclei for the formation of cloud droplets and eventually coagulate to form precipitation. Concentrations of cosmogenic radionuclides vary in the atmosphere with time and location. Variations are day-to-day, seasonal, longitudinal, and sunspot-cycle related. Annual external dose rates from cosmic rays depend slightly on latitude and strongly on altitude. Thus, at sea

level, it is approximately 340 μSv yr⁻¹. The absorbed dose rate in air from cosmic radiation outdoors at sea level is about 30 nGy h⁻¹ for the southern hemisphere [UNSCEAR, 2000].

Primordial radionuclides comprise those formed at the inception of the planet earth. Only those with half-lives comparable to the age of the earth, and their decay products, can still be found today, e.g. ^{40}K, and the radionuclides in the ^{238}U, ^{232}Th and ^{235}U decay series [Mohanty et al., 2004]. Gamma radiation from these radionuclides represents the main contributions to the external exposure of the human body. This is demonstrated especially by the gamma spectrometric analysis of the soil samples from Udagamandalam in Nilgiri District of Tamil Nadu, India [Selvasekarapandian et al., 1999; Banzi et al., 1999]. The primordial radionuclides occur in trace levels in all rocks. The specific levels of absorbed dose rate in air due to terrestrial background radiation are related to rock types. Therefore, the natural environment radiation mainly depends on geological and geographical conditions [Floron and Kritidis, 1992]. Higher radiation levels are associated with igneous rocks, such as granite, and lower levels with sedimentary rocks [Merdanoglu, B., and Altinsoy, N., 2006]. There are exceptions, however, as some phosphate rocks have relatively high content of radionuclides [UNSCEAR, 1993]. Investigations on terrestrial natural radiation have received particular attention world wide and has led to extensive surveys in many countries [UNSCEAR, 2000]. Results obtained from these countries are kept in the world's data bank and are used for evaluating worldwide average values of radiometric and dosimetric quantities. There is no systematic data on this subject for Kenya. Only a few studies on natural radioactivity and on indoor radon concentration measurements have been reported by some authors [Mangala, 1987; Patel, 1991; Mustapha, 1999; Mustapha et al., 2002].

2.4 ELEMENTAL ANALYSIS BY ENERGY DISPERSIVE X-RAY FLUORESCENCE

Energy dispersive X-ray fluorescence (EDXRF) spectrometry is used to identify elements in a sample and quantify the amount of those elements. An element is identified by the emission of its characteristic x-rays. The amount of an element present is quantified by measuring the intensity (I) of its characteristic emission [Tiwari et al., 2001]. It provides one of the simplest,

most accurate and most economic analytical methods for the determination of the chemical composition of many materials. All atoms have a fixed number of electrons arranged in orbitals around the nucleus. Energy dispersive x-ray fluorescence spectrometry typically utilizes activity in the first three electron orbitals, the K, L and M lines, where K is closest to the nucleus. EDXRF system is a powerful technique for non-destructive multi-element analysis of samples, has three major components [Bertin, 1975]: an excitation source, a spectrometer/detector, and a data collection/processing unit. In Kenya multi – elemental analysis of a variety of samples have also been carried out [Muriithi, 1982; Lavi, 1984; Mangala, 1987 e.t.c]

2.5 GAMMA DOSE ESTIMATES FROM ACTIVITY CONCENTRATIONS OF RADIONUCLIDES.

The exposure to ionizing radiation from natural radioactive sources is a continuous and un-avoidable feature of life on earth. The major sources responsible for this exposure are due to the presence of naturally occurring radionuclides in the earths crust [UNSCEAR, 1993; NCRP, 1987]. The absorbed gamma dose rates in air at 1m above the ground surface for the uniform distribution of radionuclides are computed on the basis of guidelines provided by UNSCEAR [1993, 2000]. Absorbed dose rates in air in nGy h^{-1} are computed from the dose rates in μSv h^{-1} as measured in the field using the conversion coefficient factor of 0.7 Sv Gy^{-1} as recommended by UNSCEAR (2000). Alternatively, absorbed dose rates, $\dot{D}$ (nGy h^{-1}) in air at about 1 m above ground can also be calculated from the activity concentrations of ^{232}Th, ^{238}U equivalent and ^{40}K in the soil. The conversion factors (in nGy h^{-1} per Bq/Kg) used to compute absorbed gamma dose rate in air from the activity concentration of the radionuclides in soil, are 0.621 nGy h^{-1} for ^{232}Th, 0.462 nGy h^{-1} for ^{238}U, and 0.0417 nGy h^{-1} for ^{40}K.

Based on the measured count rate under the photopeaks corresponding to the gamma-rays of ^{40}K and other radionuclides in the ^{232}Th and ^{238}U decay series, the activity concentrations of the relevant radionuclides in the samples can be determined. The procedure usually rely on the establishment of secular equilibrium between ^{226}Ra and the short lived decay products of radon in the samples [Mohanty et al., 2004]. The activity concentration of ^{232}Th is determined from

the average concentrations of ^{212}Pb and ^{214}Ac in the samples, and that of ^{226}Ra (^{238}U equivalent) is determined from the average concentrations of the ^{214}Pb and ^{214}Bi. The well known interference between the gamma lines of ^{226}Ra (186.20 keV) and ^{235}U (185.7 keV) is inevitable, especially in the presence of a relatively high uranium concentration and, therefore, the above mentioned line is not used for the determination of the activity concentration of ^{238}U equivalent [Mohanty et al., 2004].

The gamma-ray detector is normally calibrated for the energy and detection efficiency using standard sources or certified reference materials , e.g. the RG set comprising RGU-1, RGTh-1, and RGK-1, which are produced under the auspices of the IAEA and distributed through its Analytical Quality Control Services (AQCS) program.

To estimate the annual effective external dose rates, the outdoors occupancy factor is required. The value of the occupancy factor proposed by UNSCEAR (2000) is 0.2. This value is however, not representative of the area of study. In Europe and other temperate countries where a lot of time is spent indoors than outdoors, the UNSCEAR value is appropriate. For this area of study, people tend to stay outdoor for longer time due to friendly climate while attending to their daily duties. An outdoor occupancy factor of 0.4 proposed by Mustapha (1999) is more applicable.

Chapter 3

BASIC THEORY OF X-RAY FLUORESCENCE AND GAMMA – RAY SPECTROMETRY

3.1 QUANTITATIVE ANALYSIS OF SAMPLES IN EDXRF SPECTROMETRY

3.1.1 Basic x-ray intensity equation.

In x-ray fluorescence analysis, it is the intensities of the characteristic radiation from a sample, which is the basis of elemental quantitative analysis. The energy spectrum consists of the characteristic x-rays lines and background contributions due to coherent and incoherent scattering; the latter tend to interfere with quantitative analysis.

Incoherent scatter occurs when a part of the incoming x-rays is scattered by the sample instead of producing characteristic radiation. A photon hits an electron and bounces away. In this case, the photon loses a fraction of its energy which is taken away by the electron. The fraction that is lost depends on the angle at which electron was hit. On the other hand, coherent scatter happens when photons collide with strongly bound electrons. The electrons stay in their shells but start oscillating at the frequency of the incoming radiation. Due to this oscillation, the electrons emit radiation at the same frequency as the incoming radiation, which gives an impression that the incoming radiation is scattered by the atom.

Samples with light elements give rise to high incoherent scatter and low coherent scatter since they have many loosely bound electrons. For heavy elements, the incoherent scatter disappears completely and only coherent scatter remains [Brouwer, 2003]. The geometry of the excitation source in relation to the sample and the detector is shown in figure 3.1.

SOLID
DETECTOR
DIODE

VACUUM
CRYOSTAT

X-RAY TUBE

PRE-AMP

X-RAY TUBE
POWER SUPPLY

ANODE VOLTAGE
&
CURRENT CONTROLS

SLOW PULSE
SHAPING AMP

FAST AMPLIFIER

DIGITAL
COMP

DETECTOR H.V
BIAS SUPPLY

ENERGY
PULSE

REJECT

MCA

TELETYPE

LIQUID NITROGEN
DEWAR
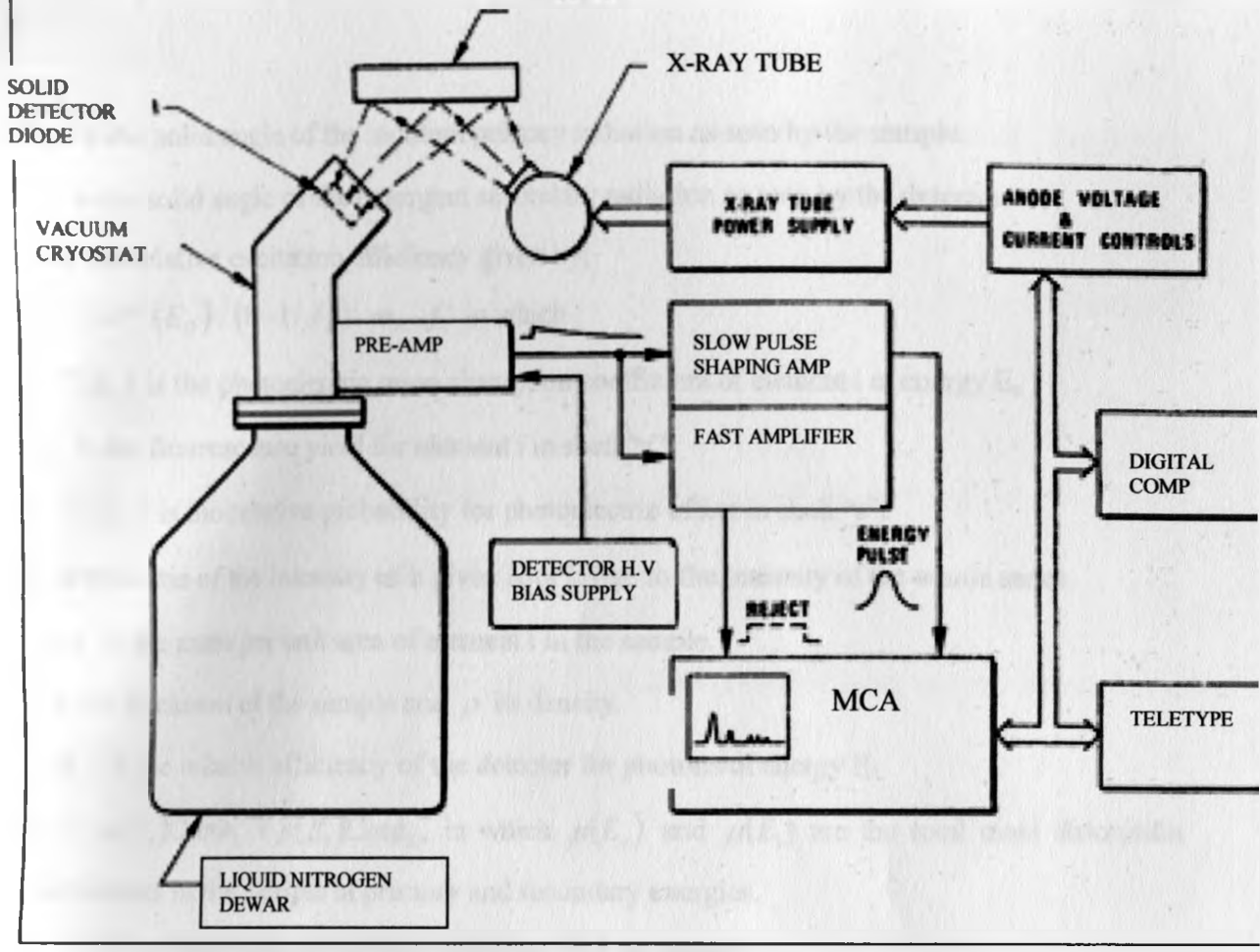
Fig.3.1: Schematic diagram of a typical x-ray tube based EDXRF spectrometer

The intensity of fluorescence radiation of element 'i' and its mass per unit area is according to Muriithi (1982), given by:

$$I_i (E_i) = G_o.K_i.\varepsilon (E_i).\rho_i d_i \left[\frac{1 - \exp(-a\rho d)}{a\rho d} \right] \qquad (3.1a),$$

where

$I_i \left(E_i \right)$ is the measured fluorescent intensity of element i.

$I_o \left(E_o \right)$ is the intensity of primary exciting radiation.

G_o is the geometry constant which is also dependent on the source activity as is the case with radioisotope sources.

$G_o = \dfrac{I_o \left(E_o \right) \Omega_1 \Omega_2}{\sin \phi_1}$ in which

13

Ω_1 is the solid angle of the incident primary radiation as seen by the sample.

Ω_2 is the solid angle of the emergent secondary radiation as seen by the detector.

K_i is the relative excitation efficiency given by;

$K_i = \sigma_i^{ph}(E_O) \cdot (1 - 1/J_{is}) \cdot \omega_{is} \cdot f_s^i$ in which

$\sigma_i^{ph}(E_o)$ is the photoelectric mass absorption coefficient of element i at energy E_0.

ω_{is} is the fluorescence yield for element i in shell "s".

$(1 - 1/j_{is})$ is the relative probability for photoelectric effect in shell "s".

f_s^i is the ratio of the intensity of a given K or L line to the intensity of the whole series.

$\rho_i d_i$ is the mass per unit area of element i in the sample.

d is the thickness of the sample and ρ its density.

$\varepsilon(E_i)$ is the relative efficiency of the detector for photons of energy E.

$A = \mu(E_o)Csc\Phi_1 + \mu(E_1)Csc\phi_2$, in which $\mu(E_o)$ and $\mu(E_1)$ are the total mass absorption coefficients in the sample at primary and secondary energies.

ϕ_1 is the incident angle of primary radiation with the sample.

ϕ_2 is the emergent angle of secondary radiation with the sample.

In the derivation of equation 3.1a, the following assumptions are made;
(i) The excitation source is considered to be a point source.
(ii) The sample is homogeneous.
(iii) The primary radiation is monochromatic.
(iv) The density of element i, ρ_i, in the sample is constant over the whole sample volume.
(v) A fixed geometry is maintained during the intensity measurements of element i in the sample, thus ϕ_1 and ϕ_2 are constant and the detector is far from the sample.

The expression $\left[\dfrac{1 - \exp(-a\rho d)}{a\rho d}\right]$ in equation 3.1a is called the absorption correction factor and it accounts for the attenuation of the primary and secondary radiation in the sample.
For thin samples, approximation of the exponential term,

14

$\exp(-a\rho d) \approx 1 - a\rho d$, with a relative error of 1% for $a\rho d \angle\angle 0.01$. Thus, equation 3.1a reduces to:

$$I_i(E_i) = G_o.K_i.\varepsilon(E_i)\rho_i d_i \qquad (3.1b)$$

in which $\rho_i d_i \leq \dfrac{0.134}{a\rho d}$. In this case the concentration in terms of the mass per unit area of element i, is linearly dependent on the fluorescence radiation intensity.

For thick samples, $\exp(-a\rho d)$ in equation (3.1a) asymptotically tends to zero for $a\rho d \gg 1$. Thus, equation (3.1a) reduces to;

$$I_i(E_i) = \dfrac{G_o.K_i.\varepsilon(E_i)\rho_i d_i}{a\rho d} \qquad (3.1c),$$

where $\rho_i d_i \geq \dfrac{0.461}{a\rho d}$.

3.1.2 Matrix effects

Matrix effects in EDXRF method consist of the influence of variations of chemical composition of the sample on the fluorescence radiation intensity of the wanted element. They constitute the major sources of errors in the method [Mangala, 1987].

There are two types of matrix effects:

(a) Absorption effect occurs when the variations in the matrix chemical composition results in changes of the mean absorption of the sample coefficients for both primary radiation and fluorescent radiation of the wanted element. Influence of these variations on $\mu_i(E_O)$ and $\mu_i(E_o)$ are evident from the intensity equation 3.1a, in which for fixed measurement conditions, the fluorescent radiation is a function of three variables;

$$I_i(E_i) = f[\rho_i d_i, \mu_i(E_o), \mu_i(E_i)] \tag{3.2}$$

(b) Enhancement effect, which consists of additional excitation of the atoms of the wanted element by the fluorescence radiation of the inter-elements. These effects constitute an ensemble of cascade processes, in which each one of them consists in excitation of the higher atoms by the fluorescence radiation of the heavier atoms. The intensity of the wanted elements will depend on the atomic numbers and the concentrations of heavier elements in the sample.

Most matrix correction methods have been developed for absorption effects since they are more dominant [Brouwer, 2003]. Enhancement effects are minimal especially when analyzing thin and diluted transparent samples of the order of $\mu g / cm^2$ or few hundreds of mg / cm^2 for most elements.

3.1.3 Matrix correction method for transparent sample analysis.

Matrix absorption effects can be experimentally determined for uniform transparent samples. The technique used involves transmission measurements of X-rays intensities from a multi-element target located at a position adjacent to the back of the sample, with and without the sample of known mass per unit area as shown in figure two below [Mangala, 1987].

(b)

Sample plus multi-element target

I_o I_{2i}

(c)

Multi-element target.

I_o I_{oi}
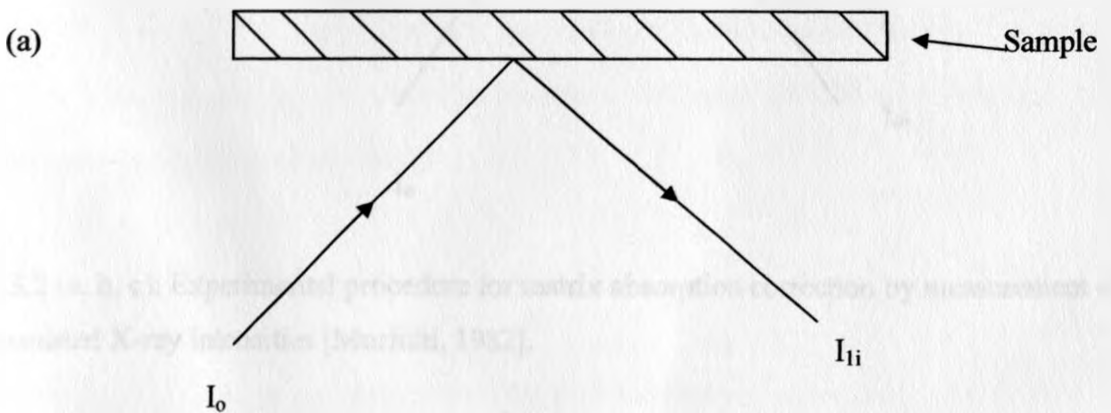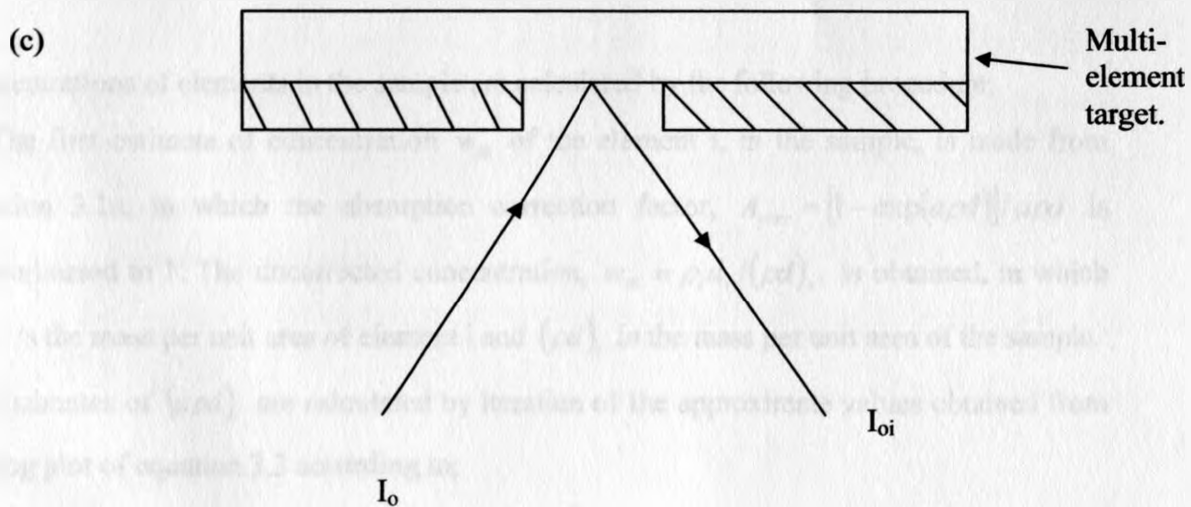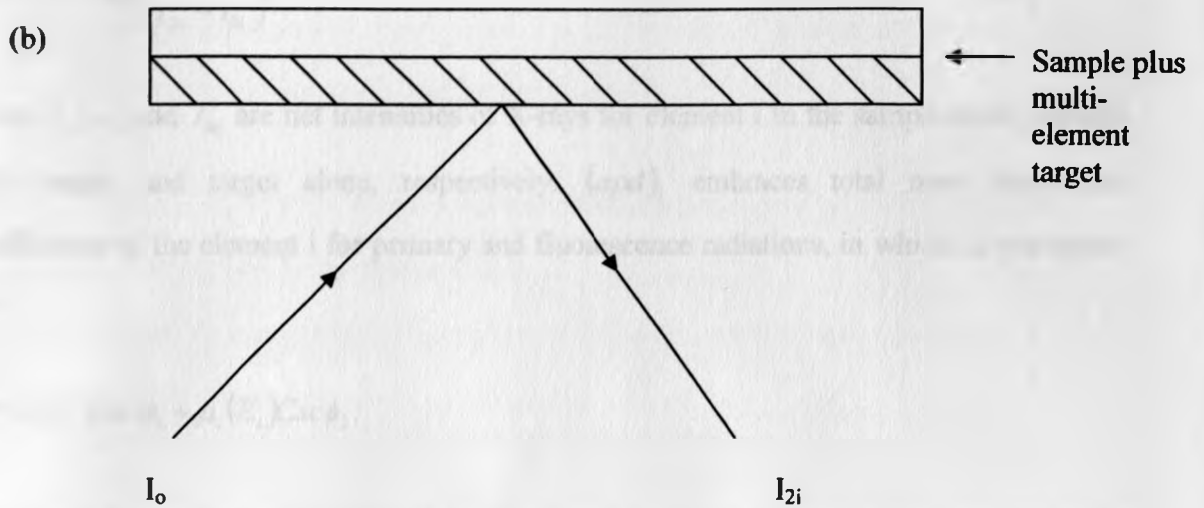
Fig.3.2 (a, b, c): Experimental procedure for matrix absorption correction by measurement of transmitted X-ray intensities [Muriithi, 1982].

The correction factor $(a\rho d)_i$ for element i due to absorption of primary and fluorescence radiations transmitted through sample of thickness $\rho d(g/cm^2)$ from the attenuation laws is given by [Muriithi, 1982].

$$(a\rho d)_i = \log_e\left(\frac{I_{0i}}{I_{2i} - I_{1i}}\right) \qquad (3.3),$$

where I_{1i}, I_{2i} and I_{0i} are net intensities of X-rays for element i in the sample alone, sample with target, and target alone, respectively. $(a\rho d)_i$ embraces total mass absorption coefficients of the element i for primary and fluorescence radiations, in which, a, was given by;

$$A = \mu_i(E_o)Csc\phi_1 + \mu_i(E_i)Csc\phi_2.$$

The multi-element target is prepared from chemical compounds whose characteristicX-rays energies are within a range of interest. Values of $(a\rho d)_i$ for elements in the target are obtained from relation (3.3) and plotted against their fluorescence x-rays energies on a log-log scale, from which aρd values of elements of interest in the sample are then interpolated.

Concentrations of elements in the sample are calculated by the following procedure;

(i) The first estimate of concentration w_{i0} of the element i, in the sample, is made from equation 3.1a, in which the absorption correction factor, $A_{corr} = [1 - \exp(a\rho d)]/a\rho d$ is approximated to 1. The uncorrected concentration, $w_{i0} = \rho_i d_i /(\rho d)_s$, is obtained, in which $\rho_i d_i$ is the mass per unit area of element i and $(\rho d)_s$ is the mass per unit area of the sample.

(ii) Estimates of $(a\rho d)_i$ are calculated by iteration of the approximate values obtained from log-log plot of equation 3.3 according to;

$$(a\rho d)_i' = (a\rho d)_i(o)[1 - (1 - 1/j_{is})w_i] \qquad (3.4),$$

in which $(a\rho d)_i(o)$ value is obtained from the presented curves on log-log scale. $(1 - 1/j_{is})$, is the relative probability for photoelectric effect in shell "s".

(iii) $(a\rho d)_i'$, from (ii) is in turn used to generate A_{Corr} factor.

(iv) The new concentration estimate, $w_i' = w_{i0} / A_{Corr}$, are substituted in equation 3.4. Steps (ii) and (iii) are repeated several times, until the difference of successive estimates of w_i' converges to less the required precision of iterations.

In cases of diluted transparent samples, the corrected concentrations w_i calculated from;

Final concentration, $w_i = w_i' \times$ dilution factor $\hspace{3cm}$ (3.5),

in which, dilution factor=(weight of sample + weight of dilutant)/weight of sample.

3.2 INTERACTION OF GAMMA RAYS WITH MATTER.

3.2.1 Gamma-ray emission

In nuclear reactions, when a nucleus decays by alpha or beta emission, the products (nuclei) are usually left in excited states. If it is energetically impossible for the excited nucleus to emit another particle, or if the decay by emission of another particle is slow, then the nucleus decays by electromagnetic interaction [Knoll, 1997]. De-excitation by electromagnetic interaction may proceed through one of the following three processes:

(i)   gamma-ray emission

(ii)   internal conversion

If the small recoil energy of the nucleus emitting the gamma-ray is neglected, the energy of the gamma-ray is given by:

$hf = \Delta E = E_i - E_f$ $\hspace{5cm}$ (3.6),

where f is the frequency of the gamma photon.

3.2.2 Selection Rules

If the angular momentum of the state of the nucleus is $\bar{J}_i$ and that of the final state is $\bar{J}_f$ then, the angular momentum carried off by th gamma photon is:

19

$$\vec{L} = \vec{J}_i - \vec{J}_f = \Delta \vec{J} \qquad (3.7),$$

in other words we have:

$$\left| J_i - J_f \right| \le L \le \left| J_i + J_f \right| \qquad (3.8),$$

$$\text{(note that } \Delta \vec{J} \ne \Delta J = \left| J_i \pm J_f \right| \text{)} \qquad (3.9),$$

Equation (ii) and (iii) imply that the vector change angular momentum $\Delta \vec{J}$ is conserved during a gamma emission. Consider a case in which the nuclear spin changes from 4 to 2 during a transition, clearly ΔJ is simply the scalar difference =2. However, $\left| \Delta \vec{J} \right|$ can have values 2, 3, 4, 5 or 6, since any integral value from 4-2 to 4+2 is possible. Obviously $\Delta \vec{J}$ for a gamma transition cannot be zero, since the intrinsic spin of the photon itself one. That is transition between two states having spin equal to zero (0→0) is forbidden.

Equation (iii) is the statement of the first selection rule. The second selection rule is that in a gamma decay, parity is always conserved, i.e. no change in parity $\Delta \pi = No$.

3.2.3 Internal Conversion

It has been mentioned that a 0→0 transition by gamma emission is forbidden (since $\Delta J = 0$ then). Therefore the other way by which a nucleus can decay from zero spin excited state to zero spin lower state is either by beta decay to form a different nuclide (a very slow process, with low probability) or it can decay more quickly by transferring the energy difference ΔE directly to a bound electron of the atom. Such an electron gets knocked out of the atom with a kinetic energy k_e given by

$$K_e = \Delta E - B_e \qquad (4.0),$$

where B_e is the electronic binding energy (of the electron), and $\Delta E = E_i - E_f$ is the nuclear excitation energy between initial state i (higher) and final state f (lower).

Electrons like these are called conversion electrons, and the process described is called internal conversion. In other words, there is no gamma emission and the excitation energy is 'converted' into ejecting an electron. The vacancy thereby created is filled by electrons from outer orbit this is accompanied by emission of x-rays. Internal conversion is most probable with electron in the K-shell, though it is also possible for other atomic shells L, M, etc.

The detection of gamma rays is based on interactions that lead to complete or partial transfer of the photon energy to an electron in the absorbing material of the detector. As a result, the photon either disappears entirely or is scattered through an angle.

The three major interaction processes known for gamma rays in matter and play an important role in radiation measurement are; photoelectric absorption, Compton scattering and pair production [Knoll, 1997].

3.2.4 Photoelectric Absorption

In this process, a photon undergoes an interaction with an absorber atom in which the photon completely disappears. The atom from one of its bound shells ejects an energetic photoelectron. The interaction is with the atom as a whole and cannot take place with free electrons. For gamma rays of sufficient energy, the most probable origin of the photoelectron is the K-shell of the atom. The photoelectron leaves the atom with an energy given by;

$$E_e = h\upsilon - E_b \tag{4.1},$$

where E_b represents the binding energy of the photoelectron in its original shell and $h\upsilon$ is the energy of the incident radiation. The photoelectron carries off the majority of the original photon energy.

The vacancy created in one of the bound shells is quickly filled through a free electron capture from the medium and/or arrangement of electrons from other shells of the atom. The photoelectric process is the predominant mode of interaction for gamma rays of relatively low energy. The probability of photoelectric absorption per atom over all ranges of E_γ and Z, is [Knoll, 1997];

21

$$\tau = Cons \tan t \times \frac{Z^n}{E_\gamma^{3.5}}$$ (4.2),

where the exponent n varies between 4 and 5 over the gamma ray energy region of interest. The dependence of photoelectric absorption probability on Z of the absorber is a major reason for preponderance of high- Z materials (e.g. lead) in gamma ray shields.

For incident photon energies greater than the k-shell electron binding energy and less than the rest mass energy of the electron, the cross-section for photoelectric emission per atom is given by;

$$\sigma_{ph} = \frac{32}{3} \sqrt{2\pi r_c^2} \, \alpha^4 z^5 \left[\frac{m_o c^2}{E_O} \right]$$ (4.3),

where r_c is the classical electron radius and α the line structure constant.

3.2.5 Compton Scattering

Compton scattering takes place between the incident gamma ray photon and an electron in the absorbing material. Compton scattering is the most predominant interaction mechanism for gamma ray energies typical of radioisotope sources. Incident gamma ray photon is deflected through an angle θ with respect to its original direction. Apportion of the energy is transferred to the electron, which is then known as a recoil electron.

22

Incident photon

Recoil electron

Φ

θ

(Energy = hυ)

Scatterd Photon
(Énergy = hυ')
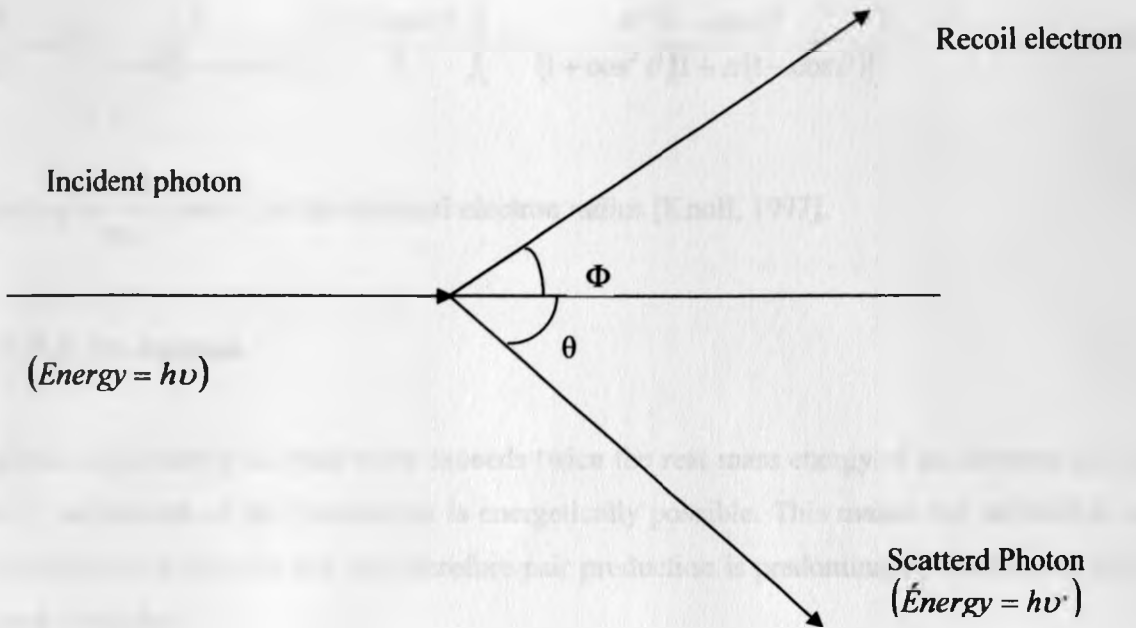
Fig.3.3: Compton scattering [Knoll, 1979].

All angles of scattering are possible hence the energy transferred to the electron, can vary from zero to a large fraction of the incident photon energy. By writing the simultaneous equations for the conservation of energy and momentum, and using the symbols defined in figure 3.3 above, it can be shown that

$$hυ' = \frac{hυ}{1 + \left(\frac{hυ}{m_o c^2}\right)(1 - \cos\theta)}$$

(4.4),

as the expression that relates energy transfer and scattering angle for any given interaction, where m_o is the rest mass of an electron and c is the speed of light .The probability of Compton scattering per atom of the absorber depends on the number of electrons available as scattering targets and thus increases linearly with Z .

The angular distribution of scattered gamma-rays is predicted by the Klein-Nishina formula for the differential scattering cross-section $\frac{d\sigma}{d\Omega}$:

23

$$\frac{d\sigma}{d\Omega} = Zr_o^2 \left(\frac{1}{1 + \alpha(1 - \cos\theta)} \right)^2 \left(\frac{1 + \cos^2\theta}{2} \right) \left(1 + \frac{\alpha^2(1 - \cos\theta)^2}{[1 + \cos^2\theta][1 + \alpha(1 - \cos\theta)]} \right) \tag{4.5},$$

where $\alpha = \dfrac{h\upsilon}{m_o c^2}$ and r_o is the classical electron radius [Knoll, 1997].

3.2.6 Pair Production

If gamma rays energy is equal to or exceeds twice the rest mass energy of an electron (0.511 MeV), the process of pair production is energetically possible. This makes the probability of this interaction to be very low and therefore pair production is predominantly confined to high gamma - energies.

In this interaction, the gamma ray photon disappears and is replaced by an electron-positron pair. The pair is created by 1.022 MeV, and all the excess energy carried in by the photon goes into kinetic energy shared by the positron and electron. Thus, two annihilation photons each of energy 0.511 MeV are normally produced as secondary products of the interaction.

No simple expression exists for the probability of pair production per nucleus, but its magnitude varies approximately as the square of the absorber atomic number.

The figure below shows the relative importance of the three major types of gamma-ray interaction. The lines show the values of Z and $h\upsilon$ for which the two neighboring effects are just equal.
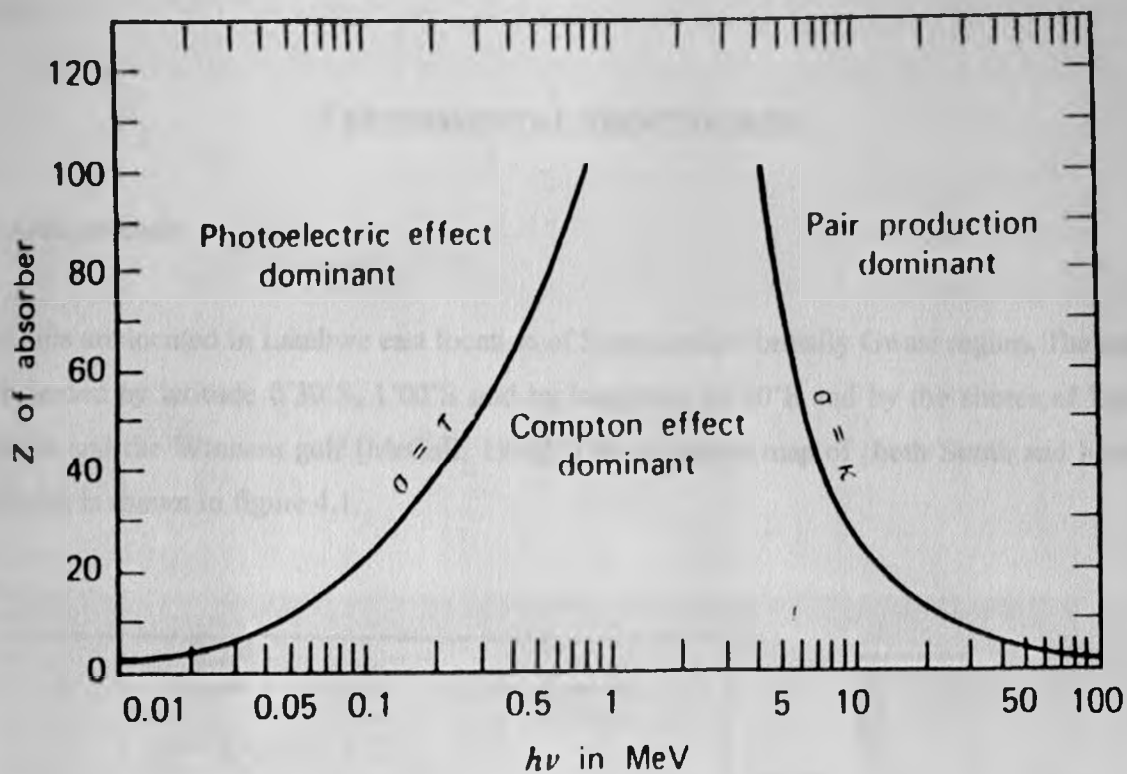
Fig3.4: The relative importance of the three major types of gamma-ray interaction [Knoll, 1997].

EXPERIMENTAL PROCEDURES

4.1 Area of study

Ruri hills are located in Lambwe east location of Suba district formally Gwasi region. The area is bounded by latitude 0˚30'S, 1˚00'S and by longitude 34˚30'E and by the shores of Lake Victoria and the Winnam gulf [McCall, 1958]. The geologica map of both South and North Ruri hills is shown in figure 4.1.

Fig. 4.1: Geology of the Ruri hills [McCall, 1958)].

The oldest rock in the Ruri hills is the Precambrian metabasalt of the Nyanzian type [McCall, 1958]. There are two types of intrusives in the Precambrian; the ijolites and nepheline syenites of tertiary age and syenodiorites of the Nyanzian age. Carbonatites of lower tertiary age form perfect ring-shaped intrusions in the Ruri hills. They are dominantly composed of calcite with iron rich segregations. These range from ferriferous carbonatites to almost pure iron-ore (magnetite-Fe_3O_4) or the "iron stone". Very often it consists of red aggregates of hematite (α-Fe_2O_3) and goethite. It is these iron-stone segregations that are associated with abnormally high radioactivity.

The high background radiation levels in the Ruri hills have been associated with the carbonatite formations [McCall, 1958]. The carbonatite rocks are rich in soda and lime in carbonated condition. They contain monazite and pyrochlore minerals, with the monazite containing principally thorium and its radioactive daughters along with several rare earth elements. Monazite is a highly insoluble rare earth mineral and its concentration in the rock or soil enhances the level of radiation. Radionuclides in monazites are from ^{232}The series, but also contain some uranium decay products e.g. ^{226}Ra.

4.2 Sampling and Sample Preparation;

Rock samples (mainly carbonatites) were collected from outcrops, particularly where the survey meter registered relatively high dose rates. A total of twenty one rock samples each weighing about 500 g was collected on both South and North Ruri hills. Figures 4.2a and 4.2b below show the sampling sites of South and North Ruri hills.

The sample preparation process comprises drying and crushing of the big boulders into smaller pieces. This is followed by pulverization with ball mills to reduce samples into fine powder of about 75 μm in size. This enhances homogeneity of the elements in the samples. About 300 g of each sample was sealed in 250 ml plastic beakers and stored for at least one month to allow for the in growth of ^{222}Rn and achievement of secular equilibrium between ^{226}Ra and decay products of ^{222}Rn before gamma spectrometric analyses [Mustapha et al., 2002]. For EDXRF

analysis, about 0.2 to 0.3 g, of each sample was pressed into a thin pellet. A total of three pellets were made from each sample.
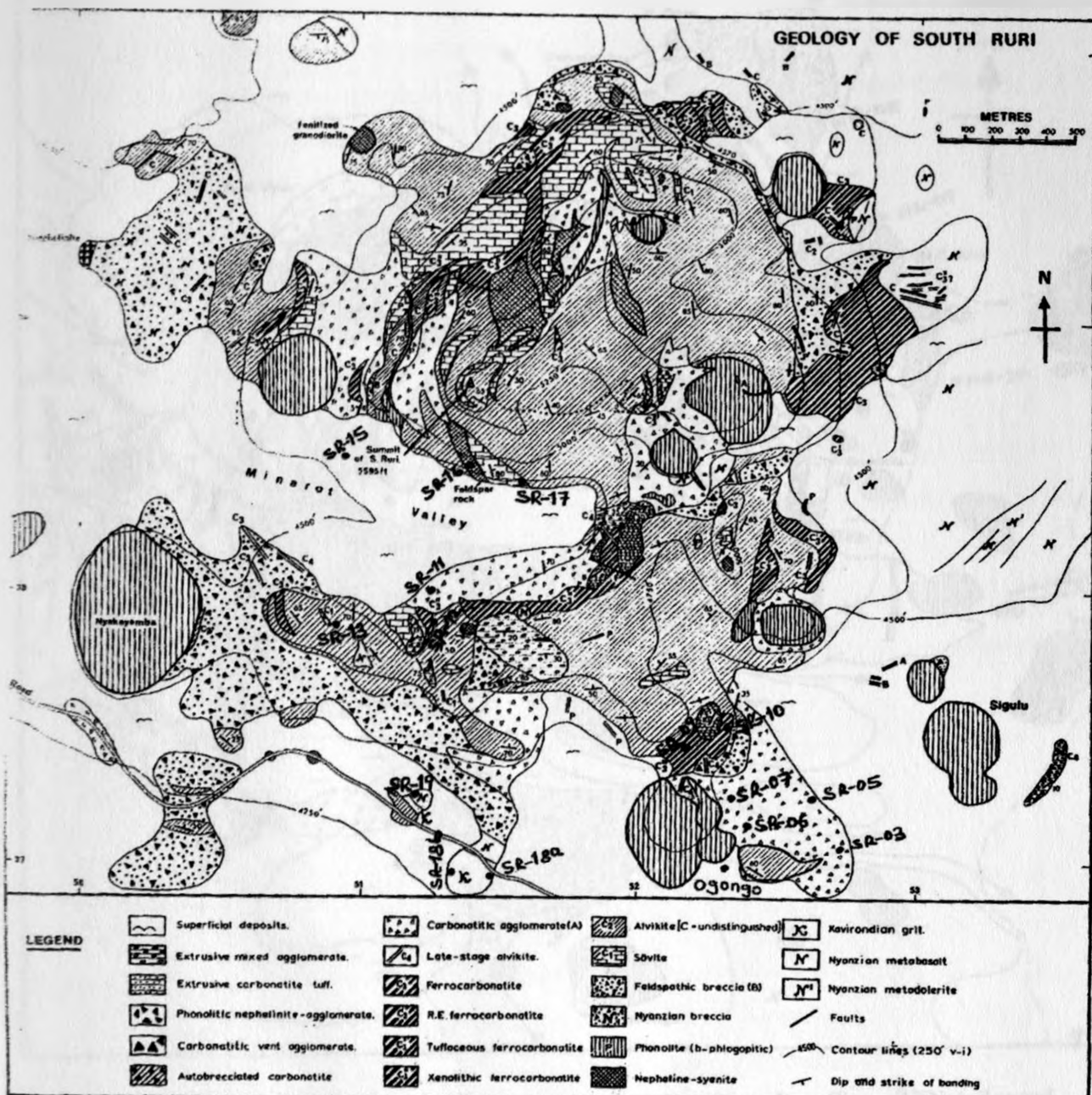

Fig. 4 .2a: Detailed geological Map of South Ruri showing sampling locations (SR) (adapted from McCall, 1958)
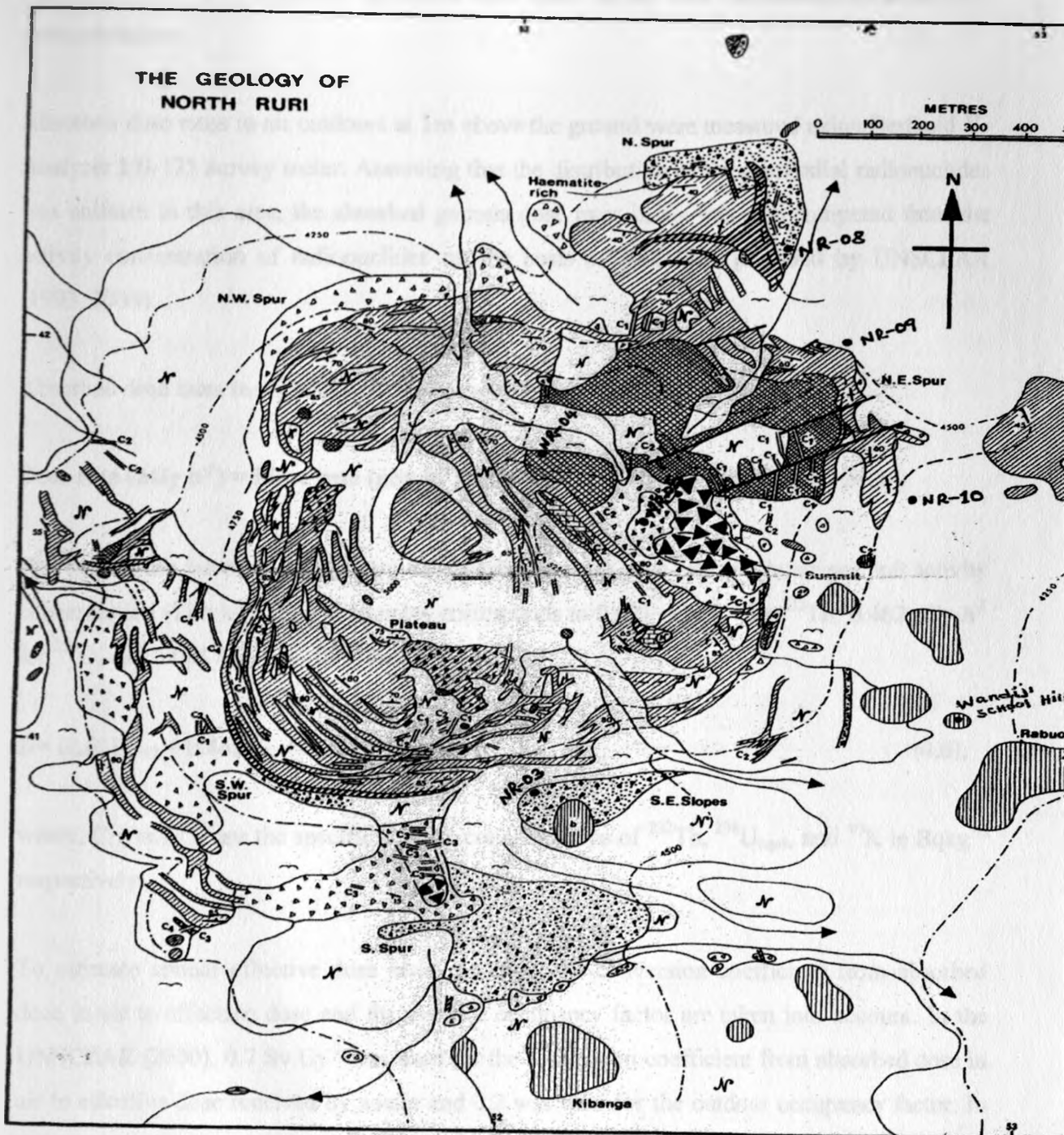
Fig.4.2b: Detailed geological Map of North Ruri showing Sampling Sites (NR) (adapted from McCall, 1958)

4.3 Measurement of external absorbed dose rates in air and Estimation from activity concentrations.

Absorbed dose rates in air outdoors at 1m above the ground were measured using Berthold Y-Analyzer LB-125 survey meter. Assuming that the distribution of the primordial radionuclides was uniform in this area, the absorbed gamma dose rates in air was also computed from the activity concentration of radionuclides on the basis of guidelines provided by UNSCEAR (1993, 2000).

Absorbed dose rates in air in $nGyh^{-1}$ are computed from the formula below;

Dose rate ($nGy\ h^{-1}$) = [dose rate ($\mu Sv\ h^{-1}$)] $\div$ (0.7 Sv $Gy^{-1} \times 10^{-3}$), [UNSCEAR, 2000].

The conversion factors used to compute absorbed gamma dose rate ($\dot{D}$) in air per unit activity concentration ($1Bq\ kg^{-1}$) in soil samples corresponds to 0.621 $nGy\ h^{-1}$ for ^{232}Th, 0.462 $nGy\ h^{-1}$ for ^{238}U, and 0.0417 $nGy\ h^{-1}$ for ^{40}K.

$$\dot{D} = (0.621C_{Th} + 0.462C_U + 0.0417C_K)\ nGy\ h^{-1} \tag{4.6},$$

where, C_U, and C_K are the specific activity concentrations of ^{232}Th, $^{238}U_{equiv}$ and ^{40}K in $Bqkg^{-1}$, respectively.

To estimate annual effective dose rates outdoors, the conversion coefficient from absorbed dose in air to effective dose and the outdoor occupancy factor are taken into account. In the UNSCEAR (2000), 0.7 Sv Gy^{-1} was used for the conversion coefficient from absorbed dose in air to effective dose received by adults and 0.2 was used for the outdoor occupancy factor. In the present research, 0.4 is used as outdoor occupancy factor [Mustapha, 1999]. Therefore, annual effective dose rate for outdoor exposure in units of $\mu Sv\ y^{-1}$ is calculated using equation 4.7.

annual effective dose rate (μSv y^{-1}) = Hourly dose (nGy h^{-1}) × 24 h per day ×365 d per year × k × 0.70 Sv Gy^{-1} ×10^{-3},   (4.7),

where k is the occupancy factor and 10^{-3} is to convert nano to micro.

4.4 HPGe Gamma-ray spectrometer

Measurement of activity concentrations of the naturally occurring radionuclides in pulverized rock samples was performed using a high-purity germanium (HPGe) gamma-ray detector with 144 ml as the active volume and outside diameter of 76 mm. The detector had an efficiency of 31.6% and a resolution of 1.8 keV at the 662 keVof ^{137}Cs or 1332 keV ^{60}Co. The detector is housed in a cylindrical lead shield. Each sample was measured for between 10-24 hours for the peaks to form (depending on the samples activity). Prior to the samples measurement, the environmental gamma background at the laboratory site was determined with an empty plastic beaker under identical measurement conditions. It was later subtracted from the measured gamma-ray spectra of each sample. The gamma-ray spectra were analyzed off line by a dedicated software program, which performs a simultaneous fit to all the significant photopeaks in the spectra. Menu driven reports are available for summaries including centroid channel, energy, net area counts, background counts, intensity and width of identified peaks in the spectrum.
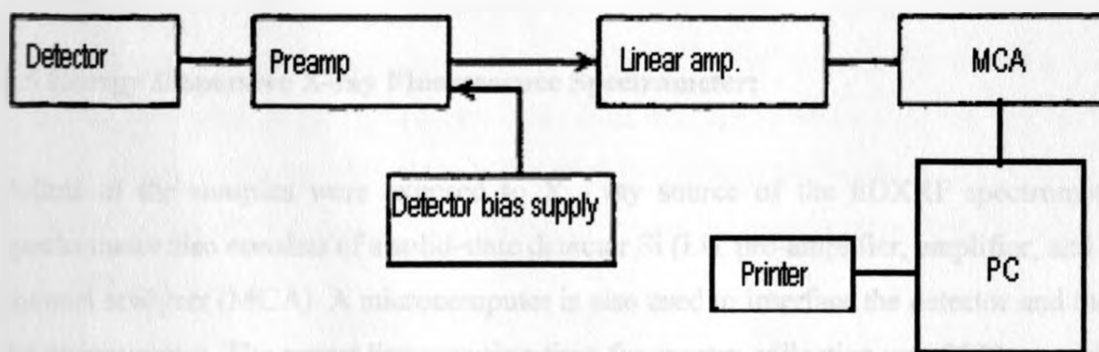

Fig.4.3: The block diagram of hyper pure germanium gamma – ray spectrometer.

31

Based on the measured gamma-ray photo-peaks emitted by specific radionuclides in the ^{232}Th series, ^{238}U equivalent decay series and in ^{40}K, their activity concentrations in the samples were determined. Calculations relied on the establishment of secular equilibrium in the samples due to the much smaller lifetime of daughter nuclides in the decay series of ^{232}Th and ^{226}Ra. More specifically, the ^{232}Th activity concentration was determined from the average concentrations of ^{212}Pb and ^{228}Ac in the samples, and that of ^{238}U equivalent was determined from the average concentrations of the ^{214}Pb and ^{214}Bi decay products. The well-known interference between the gamma lines of ^{226}Ra (186.20 keV) and ^{235}U (185.7 keV) is inevitable, especially in the presence of a relatively high uranium concentration and, therefore, the above-mentioned line was not used for the determination of the activity concentration of ^{238}U equivalent. The detector was energy calibrated using a standard source (SRM -1) supplied by the international energy atomic agency (IAEA). Certified reference materials i.e. RGU-1, RGTh-1, and RGK-1, which are produced under the auspices of the International Atomic Energy Agency (IAEA) and distributed through its Analytical Quality Control Services (AQCS) program, were sealed in the same beakers as the samples and measured for three hours each. The results obtained from the samples and those from certified reference materials were substituted in the comparative method formula to get activity concentrations of the primordial radionuclides in the samples. The comparative method formula states: $(M_sA_s \div I_s) = (M_rA_r \div I_r)$, where M_s is the mass of the sample, M_r is the mass of the reference material, I_s is the intensity of the sample, I_r is the intensity of the reference, A_s is the activity of the sample and A_r the activity of the reference material.

4.5 Energy Dispersive X-ray Fluorescence Spectrometer;

Pellets of the samples were exposed to X - ray source of the EDXRF spectrometer. The spectrometer also consists of a solid-state detector Si (Li), pre-amplifier, amplifier, and a multi-channel analyzer (MCA). A microcomputer is also used to interface the detector and the rest of the spectrometer. The preset live counting time for spectra collection was 2000 seconds for all the pellets. The resultant spectra were collected on the multi-channel analyzer in the pulse height analysis mode, and then stored on magnetic floppy diskettes for quantitative analysis.

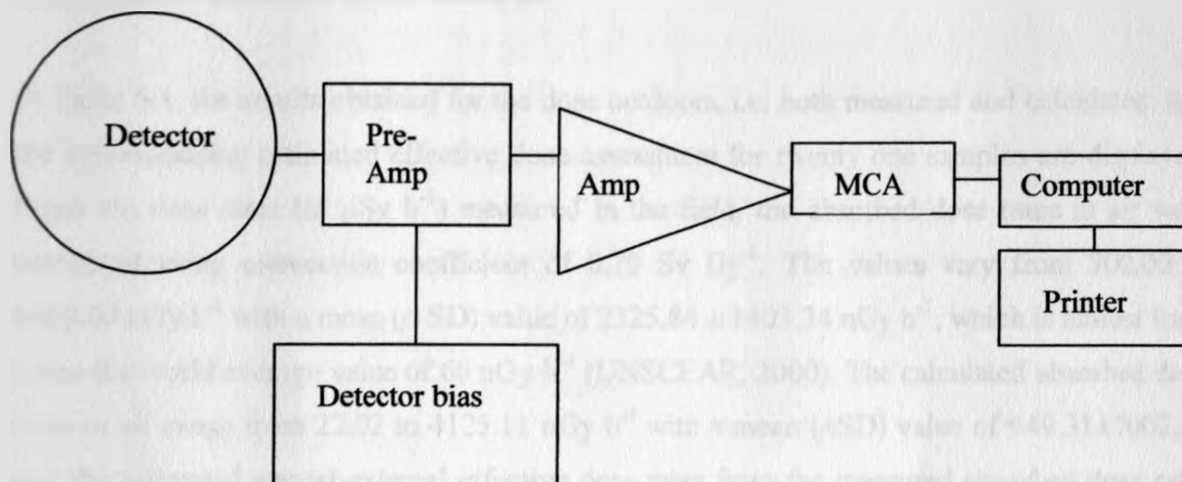The final concentration of an element is the mean of the concentrations of the element from three pellets.

Fig. 4.4: Block diagram of EDXRF spectrometry.

Pre-amplifier converts the burst of electrons, resulting from the absorption of x-rays, into electric signal, which may be conveniently transmitted to the measurement system. It also minimises any source of noise, which may degrade the resolution of the spectrum. It's located at the detector to reduce capacitance of the leads, which can degrade the rise time as well as attenuate the signal. It provides a match between the high impedance of the detector and the low impedance of the coaxial cables to the amplifier. The amplifier shapes the pulse as well as amplifies it linearly and makes the pulses suitable for the precise pulse height analysis by the multi-channel analyzer.

The multi-channel analyzer (MCA) sorts out pulses from the amplifier according to their pulse heights and accumulates the respective pulse height distribution in its memory (channels). It includes a microprocessor, which is pre-programmed to perform simple data analysis operations like energy calibration, peak integration, and subtraction of background e.tc.

33

Chapter 5

RESULTS AND DISCUSSION

5.1 Radiation absorbed dose rates in air

In Table 5.1, the results obtained for the dose outdoors, i.e. both measured and calculated; and the corresponding estimated effective dose assessment for twenty one samples are displayed. From the dose rates (in μSv h^{-1}) measured in the field, the absorbed dose rates in air were computed using conversion coefficient of 0.70 Sv Gy^{-1}. The values vary from 700.00 to 6000.00 nGy h^{-1} with a mean ($\pm$ SD) value of 2325.84 $\pm$ 1403.34 nGy h^{-1}, which is almost forty times the world average value of 60 nGy h^{-1} (UNSCEAR, 2000). The calculated absorbed dose rates in air range from 22.02 to 4125.11 nGy h^{-1} with a mean ($\pm$SD) value of 949.31$\pm$1002.23 and the estimated annual external effective dose rates from the measured absorbed dose rates vary from 1716.96 to 14716.80 μSv yr^{-1} with a mean ($\pm$ SD) value of 5704.78 $\pm$ 3442.09 μSv yr^{-1}. In this area, presence of ^{232}Th in the rocks contributed most (66%) to the total absorbed dose rate in air, followed by ^{40}K (27%) and ^{238}U (7%).

The measured external dose rates in Ruri hills are relatively higher than in some of the other high background radiation areas (HBRAs,). Examples of such high background radiation areas include the eastern coast of Orissa, India, whose values are reported to range between 650 to 3150 nGy h^{-1} with a mean value of 1925 $\pm$ 718 nGy h^{-1} and Udagamandalam, also in India whose reported value is in the range 31.6 nGy h^{-1} to 221.1 nGy h^{-1} with a mean value of 121.08 nGy h^{-1} [Selvasekarapandian et al., 1999; Mohanty et al., 2004].

34

Table 5.1: Measured and calculated radiation dose rates in air and estimated annual effective dose rates.

Sample number	Absorbed dose rates in nGy h^{-1}		Effective dose rates outdoor (μSv yr^{-1})
	Measured	Calculated	Occupancy factor = 0.4
SR-03	700 ± 14	166 ± 0.03	1717 ± 721
SR-05	871 ± 52	516 ± 0.09	2137 ± 982
SR-06	743 ± 15	110 ± 0.02	1822 ± 766
SR-07	743 ± 37	211 ± 0.38	1822 ± 820
SR-9	2857 ± 29	760 ± 0.14	7008 ± 2874
SR-10	2857 ± 29	560 ± 0.10	7008 ± 2874
SR-11	3571 ± 71	1439 ± 0.26	8760 ± 3678
SR-12	4300 ± 215	1110 ± 0.20	10547 ± 4746
SR-13	3286 ± 99	1835 ± 0.33	8059 ± 3466
SR-15	1614 ± 65	723 ± 0.13	3960 ± 1743
SR-16	4286 ± 129	3175 ± 0.57	10512 ± 4521
SR-17	871 ± 9	142 ± 0.03	2137 ± 877
SR-18A	2857 ± 57	1100 ± 0.20	7008 ± 2943
SR-18B	2857 ± 57	389 ± 0.07	7008 ± 2943
SR-19	2857 ± 29	1323 ± 0.24	7008 ± 2943
NR-03	1286 ± 129	328 ± 0.06	3154 ± 1578
NR-04	1000 ± 10	22 ± 0.01	2453 ± 1006
NR-05	2428 ± 242	485 ± 0.09	5957 ± 2976
NR-08	1000 ± 10	208 ± 0.04	2453 ± 1006
NR-09	1857 ± 371	1214 ± 0.22	4555 ± 2732
NR-10	6000 ± 600	4125 ± 0.75	14717 ± 7358
Mean	2326 ± 108	949 ± 0.19	5705 ± 2550
Stdev	1403	1002	3442

Measured absorbed dose rates in air are far much higher than the calculated absorbed dose rates. This may be attributed to the fact that the calculated values are based on the bench mark height of 1m above the ground. However, while in the field, majority of the absorbed dose rates would be measured at a height less than 1m above the ground. Again, measured absorbed dose may not have come from the sampled rock; it could have originated from somewhere else due to the effect of wind (dispersion). The sample taken may not have been a representation of what was measured in the field i.e. the measured is of different materials including what was measured in the laboratory. This implies that, the sample which was measured in the laboratory could not have been distributed homogeniously in the field.

Another reason for the difference is that, measured absorbed dose includes dose from cosmic rays i.e. both from the direct ionizing component (muons and photons) and the indirect ionizing component (neutrons). The calculated absorbed dose does not include radiation dose from cosmic rays. Dose due to external exposures to cosmic radiation at ground level was measured with Berthold LB – 125 survey meter in a boat on Lake Victoria and found to be 71.43 nGy h^{-1}. The corresponding estimated annual effective dose is 175 μSv yr^{-1} (0.175 mSv yr^{-1}).

The measured absorbed doses however, correlate positively with the calculated doses i.e. a good correlation is observed between the measured dose and the calculated dose. This is confirmed by strong positive correlation coefficient of 0.85, showing that the two doses are dependent implying that dose assessment in air can either be done through measurement or calculation. Correlation between measured absorbed dose rates and calculated absorbed dose rates is shown in Fig. 5.1.

The estimated annual effective dose rates vary from 1716.96 to 14716.80 μSv yr^{-1} with a mean (± SD) value of 5704.78 ± 3442.09 μSv yr^{-1}, which is more than that of the HBRA on the eastern coast of Orissa, India [Mohanty et al., 2004].
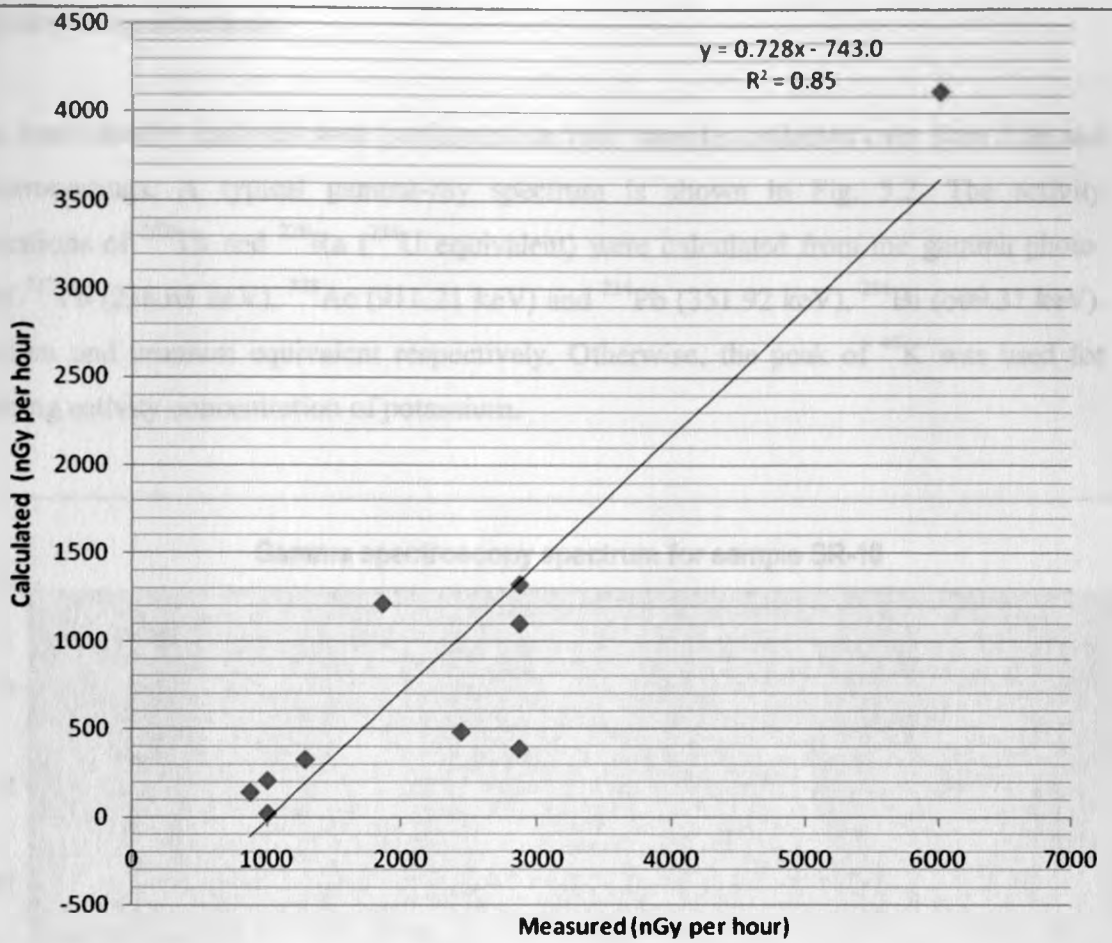
Fig. 5.1: Correlation of calculated absorbed dose in air with measured dose in air.

In normal background radiation areas, the average annual external effective dose rate from terrestrial radionuclides is approximated at 460 $\mu Sv\ yr^{-1}$ (UNSCEAR, 1993, 2000). On the basis of high levels of natural radioactivity and gamma–absorbed dose rates in air, Ruri hills regions, in Lambwe east location can be considered as high natural background radiation areas.

Absorbed dose rate in air from cosmic radiation outdoors at Ruri hills is about 71.43 $nGy\ h^{-1}$ far above 30 $nGy\ h^{-1}$, which is the value at sea level in the Southern hemisphere (UNSCEAR, 2000). The high value of absorbed dose rate in air due to cosmic radiation at Ruri hills can be attributed majorly to the altitude of the place. Lake Victoria region is about 1134 metres (3718 ft) above sea level.

5.2 Activity Concentrations

Gamma spectrometry analyses were performed on rock samples collected over Ruri hills and their surroundings. A typical gamma-ray spectrum is shown in Fig. 5.2. The activity concentrations of ^{232}Th and ^{226}Ra (^{238}U equivalent) were calculated from the gamma photo-peaks of ^{212}Pb (238.63 keV), ^{228}Ac (911.21 keV) and ^{214}Pb (351.92 keV), ^{214}Bi (609.31 keV), for thorium and uranium equivalent respectively. Otherwise, the peak of ^{40}K was used for determining activity concentration of potassium.
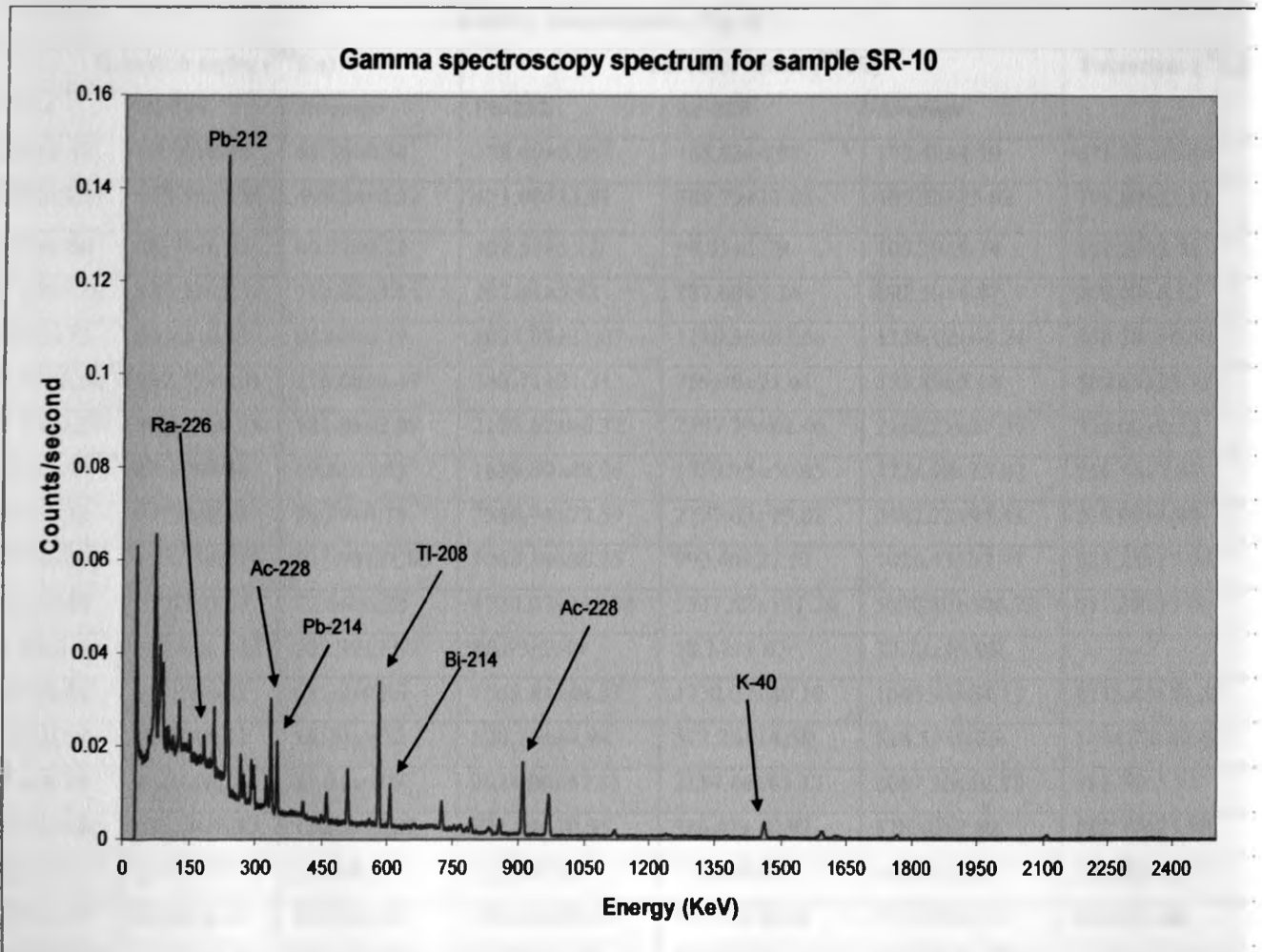

Fig. 5.2: Typical Gamma spectrum for rock sample from Ruri hills.

38

Table 5.2 gives the results corresponding to specific activities measured for the ^{232}Th series. the ^{238}U series and for ^{40}K in the rock samples collected at different locations of Ruri hills. The activity concentrations in carbonatite rock samples for ^{232}Th range from 14.18 to 6559.99 Bq kg^{-1} with an average of 1396.85 ± 1624.39 Bq kg^{-1}, for ^{238}U$_{equiv}$ range from 2.73 to 499.24 Bq kg^{-1} with a mean(±SD) of 178.69 ± 329.72 Bq kg^{-1} and for ^{40}K range from 56.67 to 1454.73 Bq kg^{-1} with an average of 508.67 ± 429.76 Bq kg^{-1}.

Table 5.2: Activity concentration of radionuclides in the samples from Ruri hills.

Sample	Activity concentration (Bq kg^{-1})						Potassium (^{40}K)
	Uranium series (^{226}Ra)			Thorium series (^{232}Th)			
	Pb-214	Bi-214	Average	Pb-212	Ac-228	Average	
SR-03	68.69±0.47	68.02±0.46	68.36±0.34	178.00±5.06	168.83±4.80	173.42±4.59	631.86±18.49
SR-05	494.92±3.31	503.55±3.36	499.24±4.32	421.00±11.91	389.75±11.03	405.38±15.63	793.69±23.11
SR-06	88.50±0.60	89.92±0.62	89.21±0.71	109.53±3.12	98.05±2.79	103.79±5.74	101.20±2.96
SR-07	175.37±1.20	182.27±1.31	178.82±3.45	197.41±5.61	187.68±5.34	192.55±4.87	209.03±6.12
SR-09	77.85±0.53	91.43±0.62	84.64±6.79	1091.88±31.07	1180.36±33.58	1136.12±44.24	358.78±10.50
SR-10	119.59±0.82	132.57±0.91	126.08±6.49	748.71±21.31	759.06±21.61	753.89±5.18	809.63±23.71
SR-11	179.54±1.07	184.32±1.25	181.93±2.39	2122.62±60.32	2197.79±62.46	2160.21±37.59	326.00±9.53
SR-12	57.22±0.39	64.47±0.44	60.85±3.63	1689.89±48.06	1759.95±50.05	1724.92±35.03	251.55±7.36
SR-13	76.02±0.52	77.52±0.53	76.77±0.75	2586.78±73.59	2777.63±79.02	2682.21±95.43	235.90±6.90
SR-15	153.80±1.05	110.15±0.75	131.98±21.83	1060.39±30.15	992.46±27.51	1026.43±33.97	583.25±17.06
SR-16	66.44±0.45	78.88±0.53	72.66±6.22	4724.07±133.88	5337.52±151.26	5030.80±306.73	411.37±12.00
SR-17	204.82±1.40	206.96±1.42	205.89±1.07	86.69±2.49	58.74±1.67	72.72±13.98	-
SR-18A	64.22±0.51	62.53±0.42	63.38±0.85	1561.81±44.33	1730.07±49.10	1645.94±84.13	1175.45±34.33
SR-18B	11.37±0.08	17.61±0.12	14.49±3.12	524.75±14.94	512.26±14.58	518.51±6.25	1454.73±42.62
SR-19	34.98±0.24	47.04±0.32	41.01±6.03	2021.06±57.35	2154.46±61.13	2087.76±66.70	181.76±5.31
NR-03	118.07±0.80	122.10±0.83	120.09±2.02	371.24±10.55	386.07±10.97	378.66±7.42	888.17±25.98
NR-04	2.62±0.02	2.84±0.02	2.73±0.11	12.75±0.36	15.60±0.44	14.18±1.43	286.62±8.37
NR-05	82.76±0.57	84.82±0.58	83.79±1.03	719.30±20.48	710.83±20.24	715.07±4.24	56.67±1.66
NR-08	267.52±1.83	275.50±1.88	271.61±4.09	137.94±3.93	97.60±2.78	117.77±20.17	111.71±3.27
NR-09	81.26±0.55	108.00±0.73	94.63±13.37	1789.52±50.76	1877.39±53.26	1833.46±43.94	758.51±22.14
NR-10	61.59±0.41	70.81±0.47	66.20±4.61	5946.45±168.42	7173.52±203.17	6559.99±613.54	498.42±14.53

The results show that apart from SR-05, SR-17 and NR-08, all the other rock samples contain higher ^{232}Th than ^{238}U equivalent (or ^{226}Ra). The Th / U ratio ranges from 0.35 in SR-17 to 99 in NR-10. Differences in the uranium and thorium contents in the rocks are attributed to the carbonatites which result to large amounts of thorium-rich monazite and pyrochlore. The differences may also be due to the large difference in the mobility of the two elements. Uranium is quite mobile as U^{+6} in oxidizing environments such as occur in shallow ground water. Thorium on the other hand is much less mobile than uranium; therefore it is more likely to remain higher in the carbonatites.

Uranium-238, though its activity concentration is generally low as compared to the other two radionuclides, seems to be uniformly distributed in this region. Thorium is sparsely distributed with activity concentration ranging from 14.18 to 6559.99 Bq kg^{-1}. The highest value of thorium content was registered at the foot of the north spur of North Ruri hill along a road bordering some homes. These samples are believed to have been deposited at the foot of the hill by erosion. Thus, they could have originated from the top of the hill. Potassium level is not as high as what is reported in other high background radiation areas e.g. Kerio Valley in Rift Valley (Mangala, 1987).

Radionuclides in samples from South and North Ruri hills do not correlate or correlate poorly (i.e. the two quantities vary separately) since correlation coefficients are either zero or near zero (figures 5.3 to 5.5). A zero correlation represents complete independence of the two quantities. Thus, there is no dependence between radionuclide content in samples from South and North Ruri hills.

The activity concentrations of radionuclides correlate positively with elemental concentrations as shown in figures 5.6 to 5.8. Correlation coefficients range from 0.35 to 0.95. In other words, measurement of elemental concentrations reveals some information on activity concentrations.
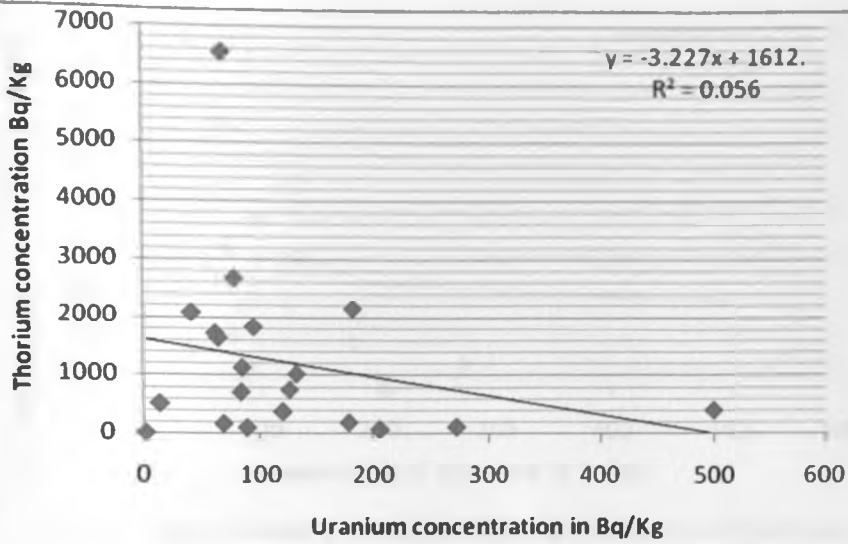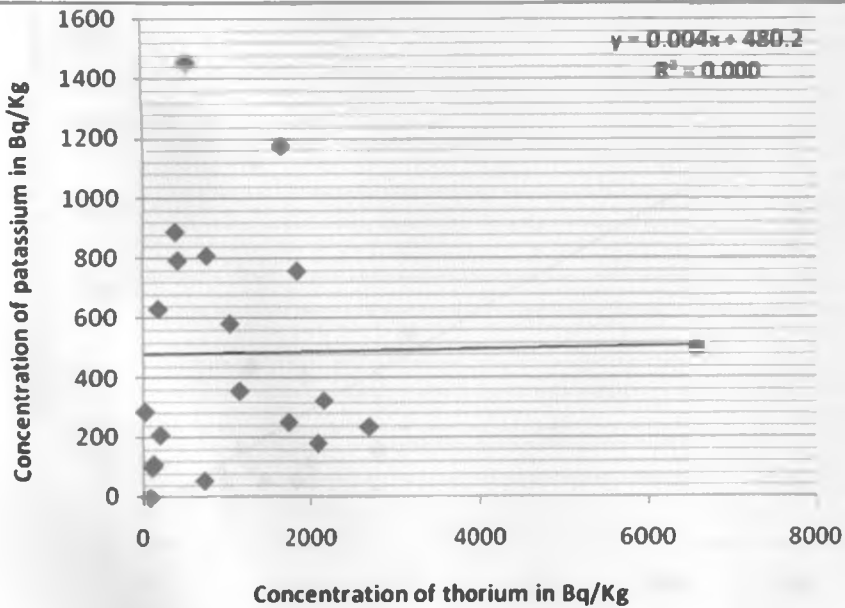
Fig. 5.3: Graph showing how thorium correlates with uranium in samples from Ruri hills.

Fig. 5.4: Graph showing correlation between potassium and thorium.
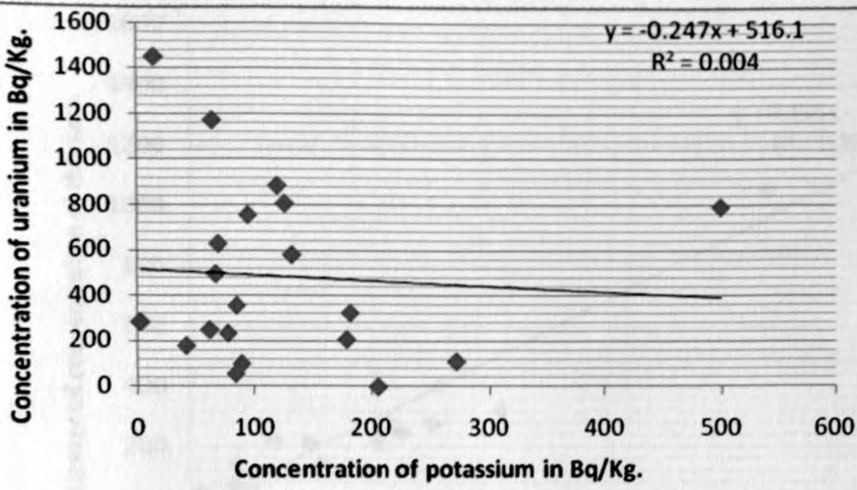
Fig. 5.5: Graph showing correlation between uranium and thorium.
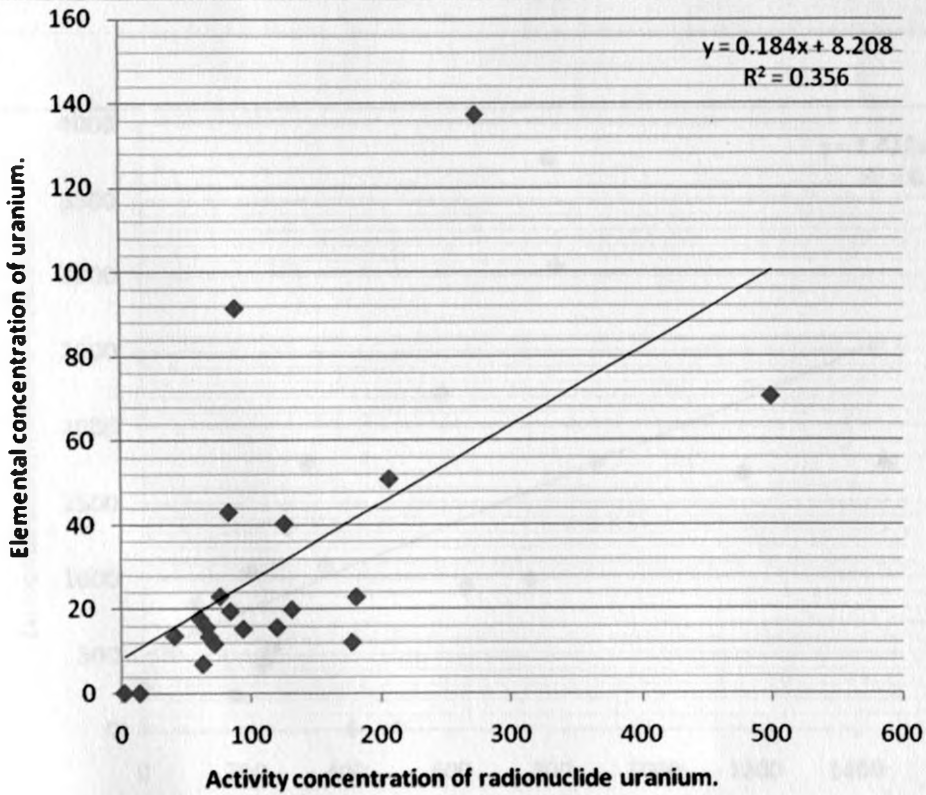

Fig. 5.6: Correlation of elemental and activity concentrations of uranium.

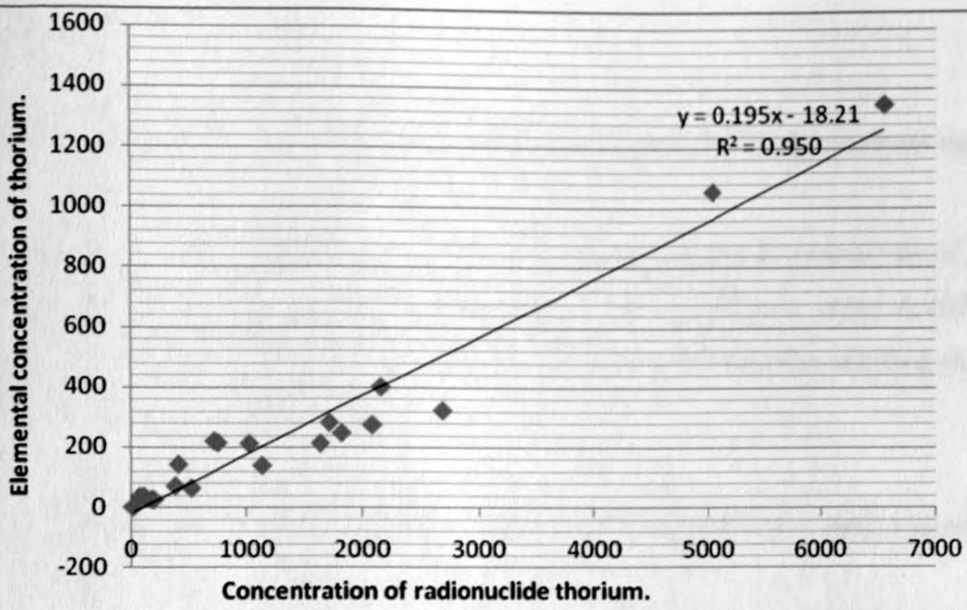Fig. 5.7: Correlation of elemental and activity concentrations of thorium.
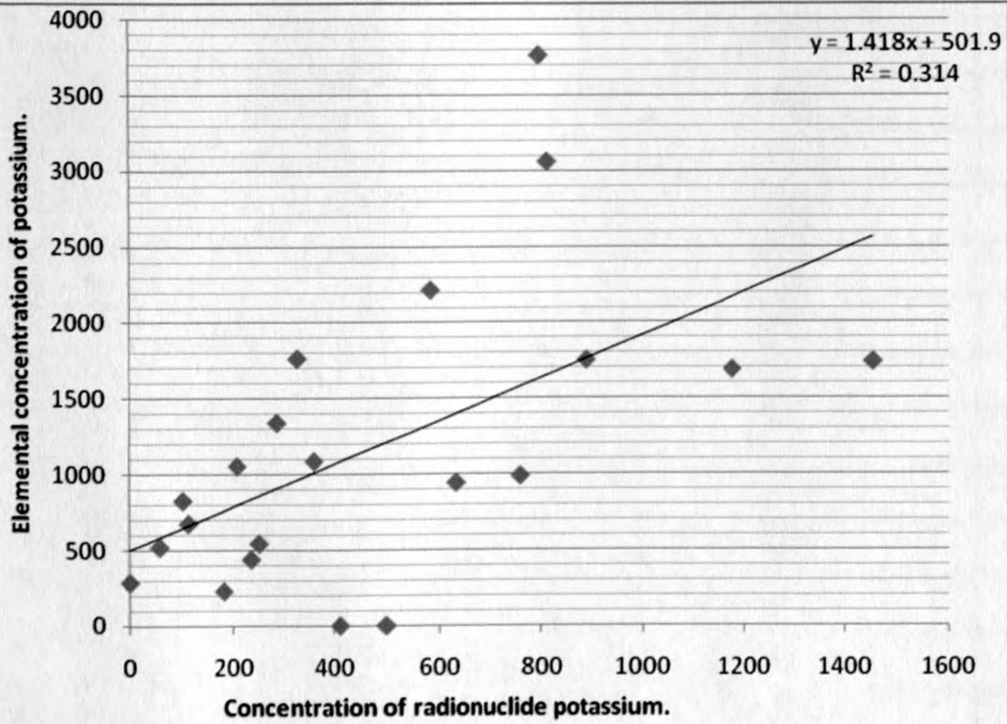
$y = 0.195x - 18.21$
$R^2 = 0.950$

Fig. 5.8: correlation of elemental and activity concentrations of potassium.

$y = 1.418x + 501.9$
$R^2 = 0.314$

5.3 Elemental Concentrations

(i) Accuracy of the energy-dispersive x-ray fluorescence (EDXRF) analysis method.

The EDXRF is a simple method for non-destructive and standardless analysis of samples (e.g. geological samples). The accuracy of the method was determined using certified reference material i.e. IAEA soil-7.The results obtained were compared with the certified values from the certificate as shown in Table 5.3 below.

Table 5.3: Results of EDXRF analysis of IAEA certified reference material soil-7

Element	Experimentally obtained values	Certified reference values (in $\mu g\ g^{-1}$ or %)	
	Concentration (in $\mu g\ g^{-1}$ or %)	Recommended concentration	Range
K	9410±700	12100*	11300 -12700
Ca	14.8%±1.4	16.3%*	(15.7 - 17.4) %
Ti	2140±500	3000*	2600 – 3700
Mn	622±20	631	604 – 650
Fe	2.31%±0.3	2.57%*	(2.52 – 2.63) %
Cu	10.6±2	11	9 – 13
Zn	94.4±7	104	101 – 113
Pb	50.7±8	60	55 – 71
Br	8.86±3	7*	3 – 10
Rb	48.7±2	51	47 – 46
Sr	115±6	108	103 – 114
Y	21.5±6	21	15 – 27
Zr	188±11	185	180 – 201
Nb	8.21±4	12*	7 – 17

* Non - certified values.

From Table 5.3, most of the concentration values agree with the certified concentration values. Small deviations are observed mostly in values which are not certified. This, therefore, demonstrates the reliability and accuracy of the EDXRF method described in this study.

Table 5.4: Average Detection Limits of identified elements.

Element	K	Ca	Ti	Mn	Fe	Zn	Rb	Sr	Y	Zr	Nb	Mo	Ce	Au	Pb	Th	U
Detection Limit (µg/g)	700	600	530	97	78	18	3	3	3	3	3	3	49	19	16	6	2.5

The detection limits of the identified elements were calculated from the formula;

$$Dl = \frac{\sqrt[3]{Bg}}{PA} \times Concentration \text{ (in µg g}^{-1} \text{ or \%)}$$
(4.8),

where Bg is the background and PA peak area [Philips, 1981].

(ii) Mean elemental concentrations of uranium, thorium and potassium.

Mean (± SD) concentrations of thorium, uranium and potassium in all the rock samples from Ruri hills are: (280.04±332.42), (27.91±21.91) and (1345.90±911.92) µg g^{-1} for thorium, uranium and potassium respectively. Table 5.5 shows total and mean elemental concentrations of these elements in all the samples. Potassium concentration is high in all the samples except in samples SR-16 and NR-10 where it could not be detected. Concentration values of potassium range from 438 µg g^{-1} to 3060 µg g^{-1}. Thorium concentration values range from 25.17 µg g^{-1} to 1346.67 µg g^{-1} and it is not detected in one sample i.e. NR-04. It exists in small quantity in eighteen samples and the concentration is relatively high in samples SR-10, SR-16 and NR-10. Uranium concentration in all the twenty one samples is generally low i.e. varying from 6.89 µg g^{-1} to 137.33 µg g^{-1}. It is not detected in samples SR-18B and NR-04.

Table 5.5: Mean concentrations of U, Th and K in rock samples from Ruri hills.

Sample Code	Element (Total concentration in µg g^{-1})		
	K	Th	U
SR-03	942.00 ± 77.93	25.17 ± 1.19	13.33 ± 1.89
SR-05	3763.33 ± 78.45	142.33 ± 5.44	70.37 ± 4.25
SR-06	825.49 ± 98.51	35.47 ± 5.11	91.47 ± 7.06
SR-07	1054.67 ± 87.73	24.27 ± 2.99	12.07 ± 1.28
SR-09	1086.67 ± 55.58	138.67 ± 15.17	19.37 ± 2.02
SR-10	3060.00 ± 130.00	214.00 ± 20.00	40.25 ± 2.35
SR-11	1763.33 ± 97.41	401.00 ± 2.16	22.80 ± 1.88
SR-12	542.67 ± 33.41	281.67 ± 4.71	17.60 ± 2.34
SR-13	438.00 ± 139.33	322.67 ± 55.22	22.95 ± 0.15
SR-15	2213.33 ± 33.00	211.67 ± 12.50	19.87 ± 4.16
SR-16	BDL	1055.67 ± 43.23	11.65 ± 1.15
SR-17	286.00 ± 27.07	34.07 ± 2.41	50.83 ±4.43
SR-18A	1686.67 ± 89.94	212.67 ± 8.50	6.89 ±0.19
SR-18B	1740.00 ± 35.59	62.93 ± 3.71	BDL
SR-19	228.00 ± 16.00	274.33 ± 15.84	13.56 ± 3.95
NR-03	1750.00 ± 56.57	70.23± 5.35	15.57 ± 1.38
NR-04	1340.00 ± 74.83	BDL	BDL
NR-05	519.00 ±135.07	220.00 ± 9.27	42.97 ± 5.38
NR-08	674.00 ± 188.87	31.70 ± 10.20	137.33 ± 0.47
NR-09	987.00 ± 74.22	247.33 ± 4.64	15.20 ± 1.51
NR-10	BDL	1346.67 ± 38.59	15.65 ± 2.05
MEAN	1345.90 ± 80.50	280.04 ± 13.31	27.91 ± 2.52
STDEV	911.92	332.42	21.91

46

Again, as observed under activity concentrations, the elemental concentrations of thorium, uranium and potassium do not correlate. There is a very poor correlation between uranium and thorium, with a correlation coefficient of 0.057; correlation of thorium and potassium is equally poor with a factor of 0.061 and lastly there is almost a zero correlation between potassium and uranium i.e. correlation factor is 0.001. Therefore uranium, thorium and potassium are independent of each other in these areas of study. Presence of one element may not necessarily mean that the other is also present in the same or comparable amount. Figures 5.9 to 5.11 show how the three radionuclides correlate with each other.
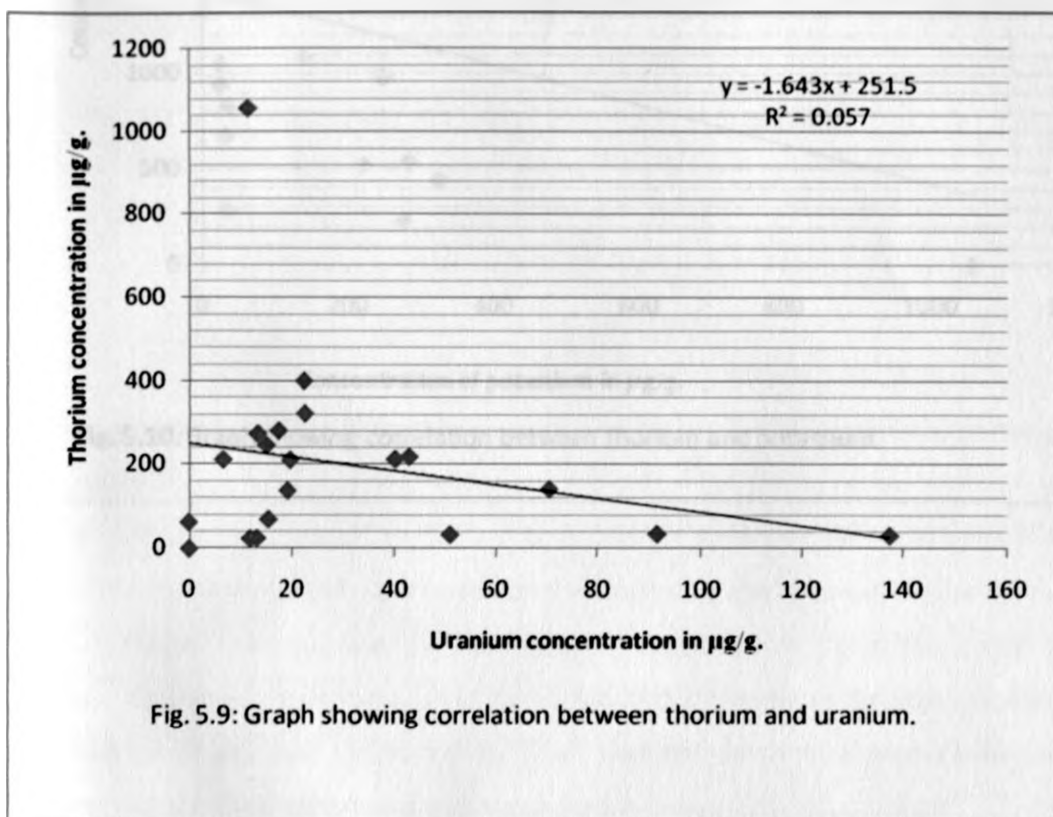

$$y = -1.643x + 251.5$$
$$R^2 = 0.057$$

Fig. 5.9: Graph showing correlation between thorium and uranium.

47

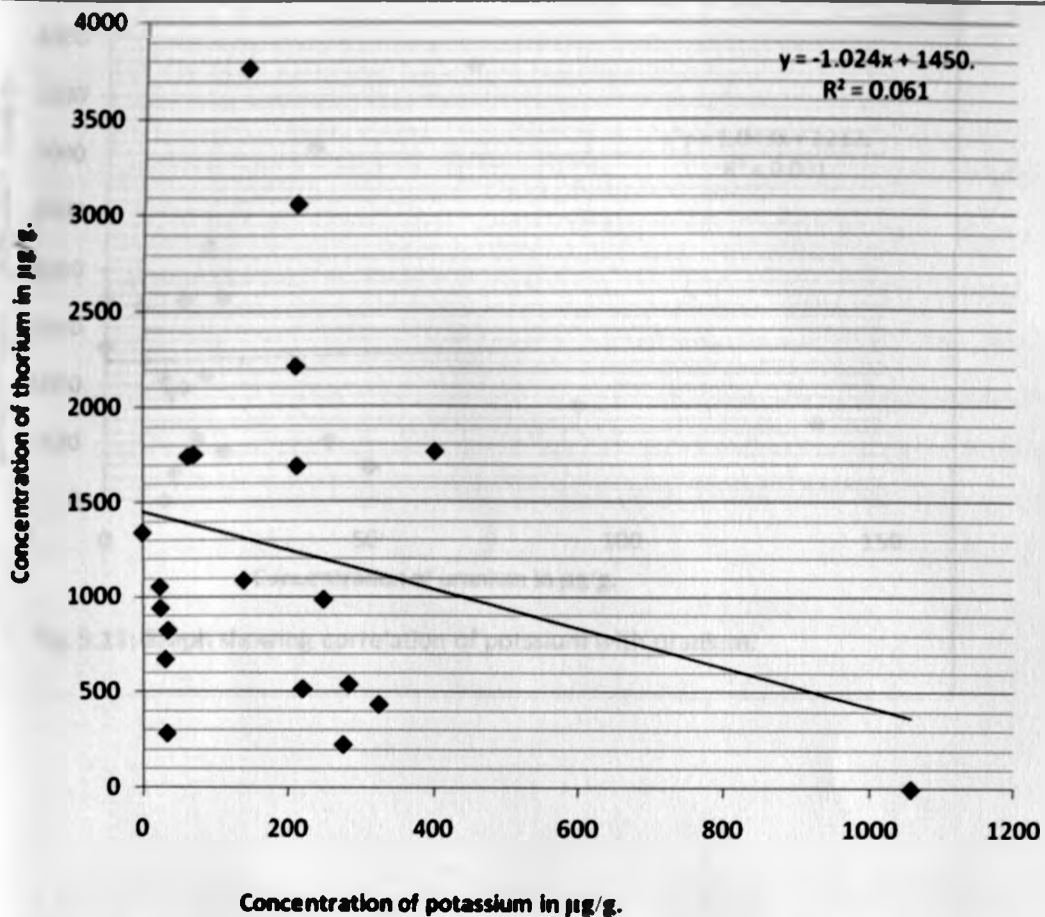Fig. 5.10: Graph showing correlation between thorium and potassium.

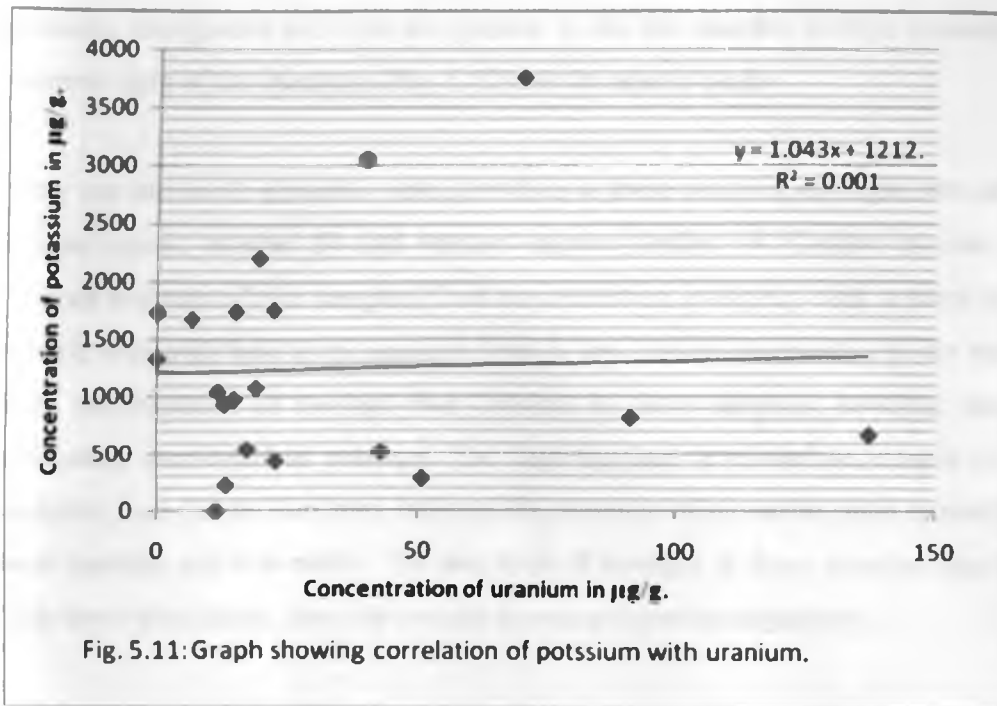Fig. 5.11: Graph showing correlation of potssium with uranium.

Table 5.6 contains X-Ray fluorescence analysis results of rock samples from South Ruri hill. Samples analyzed from this area were predominantly carbonatite rocks. The concentrations of all the elements are reported in Table 5.6. A total of seventeen elements were identified and quantified. In some samples, the concentration of certain elements was low and hence reported as BDL (below detection limits). The identified elements are; potassium, calcium, titanium, cerium, manganese, iron, zinc, gold, lead, rubidium, strontium, thorium, yttrium, uranium, zirconium, niobium, and molybdenum. These elements occur in almost all the samples. The elements of the three primordial radionuclides i.e. potassium- 40, thorium- 232 and uranium-238, occur in all the samples but in small quantities. Potassium and thorium seem to correlate negatively such that in samples where potassium is present in high concentration, thorium level is low and vice versa. A similar relationship is witnessed between calcium and iron. The concentration of calcium is high in all the samples from South Ruri hills. Gold is uniformly distributed in this region going by the registered concentrations. Figure 5.12 shows a typical fluorescence spectrum of a SR-10 sample from South Ruri hill. It is noted that calcium,

49

titanium, manganese and iron are present in all the samples in high concentrations. At the extreme right of the spectrum (Fig. 5.12) are the scatter peaks.

Only two rare earth elements were identified in these samples; one light rare earth element i.e. cerium atomic number 57 and yttrium atomic number 39. Cerium is more abundant than yttrium in almost all the samples. Lead concentration is slightly high in some samples and in a sample with high lead level, uranium level is low, this is observed in all the samples. There is high concentration of thorium than uranium in these samples; however, thorium is not as uniformly distributed as uranium. The high thorium level and occurrence or rare earths in samples from South Ruri may indicate the presence of monazite since monazite is associated with thorium and rare earths. The low level of uranium in these samples may be attributed to high level of calcium, since the two are known to correlate negatively.

Table 5.6: XRF results of carbonatite rock samples from South Ruri hills.

Element	Mean elemental concentrations in rock samples from South Ruri hill				
	Laboratory code numbers of samples.				
	SR-03	SR-05	SR-06	SR-07	SR-09
K	942.00 ± 77.93	3763.33±8.45	825.49 ± 98.51	1554.67±87.73	1786.67±55.58
Ca	(20.83±0.39)%	(4.92±0.07)%	(80.00±2.94)%	(14.70±0.45)%	(32.40±0.37)%
Ti	5220.00±375.59	(2.16±0.02)%	BDL	5153.33±403.02	2710.00±149.89
Mn	3713.33±93.7	(2.54±0.02)%	(1.40±0.05)%	2430.00±184.03	(1.69±0.02)%
Fe	(4.49±0.12)%	(45.43±0.49)%	(4.07±0.21)%	(4.26±0.19)%	(3.40±0.07)%
Zn	221.33±6.18	1850.00±29.44	1090.00±43.20	166.00±5.66	471.67±20.95
Au	24.63±1.19	70.63±14.31	96.20±5.51	19.83±3.07	47.73±6.93
Pb	48.63±3.00	399.00±34.65	169.67±6.94	41.47±5.56	165.67±4.50
Rb	56.87±1.16	164.67±1.70	26.10±5.59	57.67±2.22	44.80±4.12
Sr	1603.33±24.94	914.67±18.84	5903.33±236.13	1306.67±44.97	3046.67±55.58
Th	25.17±1.19	142.33±5.44	35.47±5.11	24.27±2.99	138.67±15.17
Y	40.40±2.33	119.33±6.13	183.33±10.21	39.00±1.56	248.00±9.20
U	13.33±1.89	70.37±4.25	91.47±7.06	12.07±1.28	19.37±2.02
Ce	1293.33±121.20	BDL	8270.00±531.60	1853.33±732.77	5303.33±918.56
Zr	180.67±4.11	968.33±21.70	50.40±7.02	160.67±7.13	95.83±21.34
Nb	277.67±4.19	3020.00±69.76	1443.33±44.97	371.00±11.43	387.33±17.99
Mo	3.27±1.52	33.17±2.54	8.27±1.54	5.87±2.86	22.33±1.68

N/B: Concentration values are in $\mu g \ g^{-1}$, unless otherwise stated.

Table 5.6 continued:

Element	Mean elemental concentrations in rock samples from South Ruri hill				
	Laboratory code numbers of samples.				
	SR-10	SR-11	SR-12	SR-13	SR-15
K	3060.00±130.00	1763.33±97.41	BDL	BDL	2213.33±33.00
Ca	(36.15±1.55)%	(7.94±0.08)%	(35.83±0.25)%	(36.93±1.09)%	(2.09±0.09)%
Ti	7445.00±235.00	(1.01±0.01)%	BDL	BDL	6253.33±279.21
Ce	8075.00±465.00	(1.02±0.03)%	(0.96±0.07)%	5923.33±479.33	3156.67±268.49
Mn	(2.05±0.08)%	(3.01±0.02)%	(1.56±0.03)%	(2.10±0.03)%	(1.13±0.06)%
Fe	(13.10±0.80)	(10.90±0.08)%	(2.93±0.01)%	(1.72±0.04)%	(9.32±0.53)%
Zn	1022.50±57.5	935.00±18.83	684.33±8.73	450.67±4.03	740.67±54.36
Au	87.35±4.75	49.60±7.74	60.17±3.23	62.80±5.09	19.73±1.97
Pb	232.50±16.50	352.33±10.40	306.33±7.72	201.33±19.87	271.00±17.91
Rb	159.00±12.00	131.33±0.94	37.77±1.68	BDL	111.67±3.77
Sr	3535.00±205.00	1783.33±12.47	3190.00±16.33	4383.33±106.25	460.33±20.24
Th	214.00±20.00	401.00±2.16	281.67±4.71	322.67±55.22	211.67±12.50
Y	242.00±9.00	460.00±6.68	548.00±2.16	489.00±7.07	152.33±7.93
U	40.25±2.35	22.80±1.88	17.60±2.34	22.95±0.15	19.87±4.16
Zr	417.00±21.00	360.33±60.14	237.33±2.62	BDL	374.00±17.28
Nb	759.00±29.00	790.33±7.41	329.67±2.05	205.67±6.85	772.00±40.01
Mo	13.90±0.60	BDL	20.57±1.11	11.25±0.05	16.47±1.40

N/B: Concentration values are in $\mu g\ g^{-1}$, unless otherwise stated.

Table 5.6 continued:

Element	Mean elemental concentrations in rock samples from South Ruri hill				
	Laboratory code numbers of samples.				
	SR-16	SR-17	SR-18A	SR-18B	SR-19
K	BDL	BDL	1686.67±89.94	1740.00±35.59	BDL
Ca	(2.99±0.03)%	(35.77±1.27)%	(1.73±0.07)%	5050.00±423.40	(12.00±0.08)%
Ti	5073.33±865.54	BDL	4460.00±99.33	3283.33±244.18	3700.00±225.54
Ce	7500.00±266.96	BDL	3263.33±179.69	915.00±227.80	4363.33±463.49
Mn	(7.40±0.17)%	5520.00±264.70	(1.95±0.04)%	1466.67±148.17	(2.99±0.07)%
Fe	(48.00±1.31)%	(8.56±0.22)%	(22.20±0.36)%	(2.93±0.20)%	(17.90±0.51)%
Zn	1723.33±87.31	303.00±25.15	661.33±25.49	132.00±8.60	1176.67±52.49
Au	67.33±17.19	34.37±10.21	59.73±4.50	17.85±1.95	67.60±10.90
Pb	1020.00±16.33	56.20±9.95	885.33±158.87	93.63±3.36	1137.67±41.10
Rb	13.65±1.35	BDL	56.33±2.50	73.57±6.62	BDL
Sr	827.00±27.53	1696.67±82.19	494.33±5.19	146.00±11.22	472.00±17.28
Th	1055.67±43.25	34.07±2.41	212.67±8.50	62.93±3.71	274.33±15.84
Y	145.67±5.56	41.60±2.03	241.00±3.74	42.13±1.72	123.33±4.64
U	11.65±1.15	50.83±4.43	6.89±0.19	BDL	13.56±3.95
Zr	119.00±4.32	146.67±7.85	253.67±12.97	119.33±8.99	BDL
Nb	355.67±11.02	521.33±8.73	228.00±1.41	110.90±10.35	17.47±0.65
Mo	34.87±2.66	BDL	4.52±0.01	BDL	81.97±2.65

N/B: Concentration values are in µg g^{-1}, unless otherwise stated.

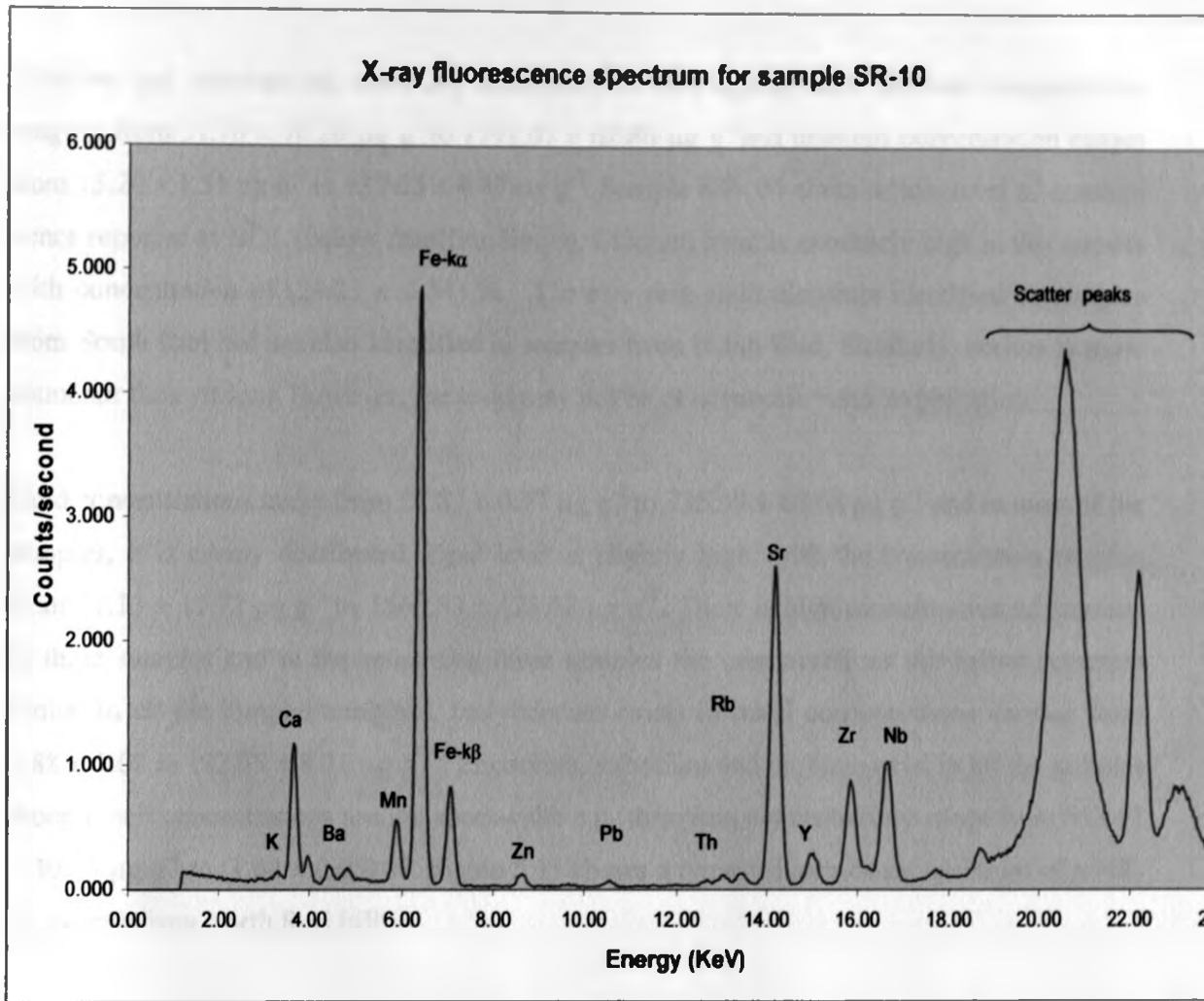## X-ray fluorescence spectrum for sample SR-10

Fig. 5.12: A typical EDXRF spectrum of SR-10 sample from South Ruri hill.

Table 5.7 shows X-ray fluorescence analysis results of rock samples from North Ruri hill. The major constituents in these samples are calcium and iron. A total of seventeen elements have been identified in these samples. The results of their concentration values are reported in Table 5.7. Potassium occurs in five out of six samples from North Ruri hill. It exists in lower concentration in sample number ten i.e. NR-10, where thorium concentration is highest i.e. 1791.07 ± 62.86 µg g⁻¹. In sample number three (NR-03), where potassium concentration is

highest, the concentrations of thorium and uranium are very low e.g. 70.23 ± 5.35 µg g^{-1} and 15.57 ± 1.38 µg g^{-1} respectively.

Thorium and uranium are unevenly distributed in this region, with thorium concentration ranging from 31.70 ± 10.20 µg g^{-1} to 1791.07 ± 62.86 µg g^{-1} and uranium concentration ranges from 15.20 ± 1.51 µg g^{-1} to 137.33 ± 0.47 µg g^{-1}. Sample NR- 04 contains low level of uranium hence reported as BDL (below detection limits). Calcium level is extremely high in this sample with concentration of (24.23 ± 1.54) %. The two rare earth elements identified in samples from South Ruri hill are also identified in samples from North Ruri. Similarly, cerium is more abundant than yttrium. However, the level may not be of economic value exploitation.

Gold concentrations range from 27.87 ± 0.77 µg g^{-1} to 135.39 ± 68.08 µg g^{-1} and in most of the samples, it is evenly distributed. Lead level is slightly high, with the concentration ranging from 81.13 ± 11.72 µg g^{-1} to 1560.53 ± 123.58 µg g^{-1}. There is high concentration of titanium in three samples and in the remaining three samples the concentrations are below detection limits. In all the samples analyzed, molybdenum exists in small concentrations varying from 5.88 ± 1.08 to 182.65 ± 8.02 µg g^{-1}. Zirconium, strontium and niobium exist in all the samples though their concentrations are not spectacular e.g. strontium concentrations range from 653.67 ± 30.18 µg g^{-1} to (1.64 ± 0.05) %. Figure 5.13 shows a typical fluorescence spectrum of a NR-03 sample from North Ruri hill.

Table 5.7: XRF results of carbonatite rock samples from North Ruri hill.

Element	Mean elemental concentrations in rock samples from North Ruri hill				
	Laboratory code numbers of samples.				
	NR-03	NR-04	NR-05	NR-08	NR-09
K	1750.00±56.57	1740.00±74.83	BDL	BDL	1987.00±74.22
Ca	(6.50±0.14)%	(24.23±1.54)%	(78.90±1.79)%	(77.07±7.45)%	(7.68±0.30)%
Ti	6296.67±234.71	(1.60±0.13)%	BDL	BDL	5453.33±70.40
Ce	1926.67±98.77	BDL	7276.67±533.25	5266.67±987.57	2710.00±160.83
Mn	6996.67±74.09	4986.67±349.89	(6.22±0.10)%	(1.11±0.12)%	(1.37±0.05)%
Fe	(7.20±0.08)%	(18.2±1.13)%	(4.65±0.10)%	(5.86±0.57)%	(8.01±0.23)%
Zn	361.00±1.41	298.67±59.16	700.00±11.05	249.67±11.47	446.00±19.44
Au	27.87±0.77	55.90±6.87	88.07±10.28	124.00±10.71	37.63±0.78
Pb	114.00±1.41	84.47±13.55	526.33±13.72	81.13±11.72	229.33±5.31
Rb	83.57±2.44	39.67±1.97	BDL	31.53±2.67	53.47±1.32
Sr	849.33±7.13	653.67±30.18	7196.67±59.07	(1.64±0.05)%	1456.67±41.10
Th	70.23±5.35	BDL	220.00±9.27	31.70±10.20	247.33±4.64
Y	99.00±1.21	30.30±1.71	750.33±15.37	150.00±5.10	191.67±5.31
U	15.57±1.38	BDL	42.97±5.38	137.33±0.47	15.20±1.51
Zr	399.67±10.37	87.57±1.78	37.75±0.35	BDL	239.00±7.48
Nb	437.67±7.32	25.33±1.09	128.00±0.82	386.00±9.93	361.33±13.82
Mo	14.57±0.85	BDL	33.33±0.77	5.88±1.08	23.10±0.43

Table 5.7 continued:

Element	Mean elemental concentrations in rock sample
	Laboratory code number of sample.
	NR-10
K	BDL
Ca	(9.60±0.48)%
Ti	BDL
Ce	(1.58±0.08)%
Mn	(12.62±0.82)%
Fe	(58.96±4.11)%
Zn	2615.67±201.42
Au	135.39±68.08
Pb	1560.53±123.58
Rb	BDL
Sr	3085.60±140.75
Th	1791.07±62.86
Y	600.72±15.12
U	20.81±3.86
Zr	219.89±12.78
Nb	243.88±6.69
Mo	182.65±8.02

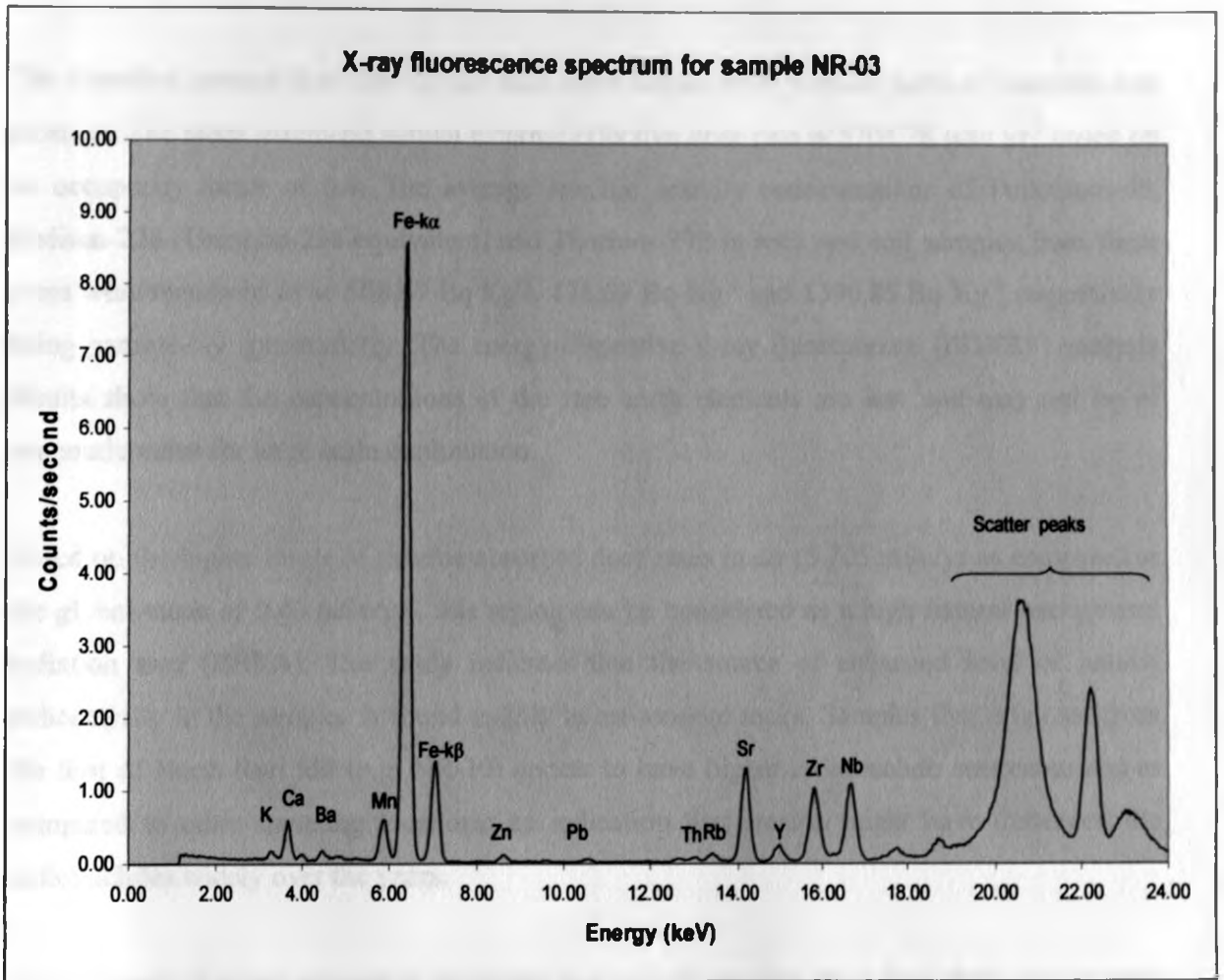N/B: Concentration values are in $\mu g\ g^{-1}$, unless otherwise stated.

Fig. 5.13: A typical EDXRF spectrum of NR-03 sample from North Ruri hill

CONCLUSIONS AND RECOMMENDATIONS

The absorbed gamma dose rates in air have been measured in various parts of Lambwe east location. The mean estimated annual external effective dose rate is 5704.78 µSv yr⁻¹ based on an occupancy factor of 0.4. The average specific activity concentrations of Potassium-40, Radium-226 (Uranium-238 equivalent) and Thorium-232 in rock and soil samples from these areas were measured to be 508.67 Bq Kg⁻¹, 178.69 Bq Kg⁻¹ and 1396.85 Bq Kg⁻¹ respectively using gamma-ray spectrometry. The energy-dispersive x-ray fluorescence (EDXRF) analysis results show that the concentrations of the rare earth elements are low and may not be of economic value for large scale exploitation.

Based on the higher levels of gamma-absorbed dose rates in air (5.705 mSv/yr as compared to the global mean of 0.46 mSv/yr), this region can be considered as a high natural background radiation area (HBRA). The study indicates that the source of enhanced level of natural radioactivity in the samples is found mainly in carbonatite rocks. Samples that originate from the foot of North Ruri hill (e.g. NR-10) appear to have higher radionuclide concentrations as compared to other sampling locations; an indication that erosion might have dispensed the radionuclides widely over the years.

This research has not exhausted elemental analysis of samples from Ruri hills and as such further research should be done especially on the analysis of water samples from existing rivers and boreholes. Soil samples from homesteads and farm lands should also be analyzed so that the correlation between elemental concentrations in soil and rock samples in these areas can therefore be established.

In view of the radiation level of Ruri hills and its environ, it is recommended that more radiological research be done in this area especially on the measurement of indoor radon concentration, radon level in water from the boreholes and on the health implications of the

high radiation levels on the residents. For instance, an epidemiological study of the inhabitants of both high and normal background radiation areas of Ruri hills should be embarked upon.

I would also recommend that the Radiation Protection Board be involved in future further radiological studies to implement any necessary professional steps for the good of the residents and the nation as a whole. Emphasis should be put on the measured and calculated values of radiation dose rates to address the huge variations between the two reported dose rates.

REFERENCES

Ajlouni, A.; Abdesalam, M.; Osama, A.; Joude, B. (2009) A very high natural radiation area in Afra hot springs. Radiat. Prot. Dosimetry 133(2): 115 – 118.

Akhtar, N., Tufail, M., Ashraf, M., (2005) Natural environmental radioactivity and estimation of radiation exposure from saline soils. International Journal of Environmental science and Technology, **1 (4):** 279-285.

Banzi, F. P., Kifanga, L. D., Bundala, F. M., (1999) Natural radioactivity and radiation exposure at the Minjingu phosphate mine in Tanzania, J. Radiol. Prot. **20:** 41-51.

Bear, L. M. (1952) Soil samples from Homa Mountains and Ruri areas, filed report, Mines and Geology Department, Ministry of Natural Resources, Government of Kenya, Nairobi.

Bertin, P. E. (1975) Principles and Practice of X-ray Spectrometric Analysis, Plenum Press, New York, 529-545.

Brouwer, P. (2003) Theory of XRF; Getting acquainted with the principles, PAN analytical B.V., Netherlands, Almelo.

Deer, W. A., Howie, R.A. and Zussman, J. (1995) An Introduction to the Rock-forming Minerals, Longman, Essex.

Edsfeldt, C. (2001) The Radium distribution in some Swedish soils and its effect on radon emanation, Ph.D thesis, Royal Institute of Technology, Published.

Freital, A. C. and Alencar, A. S. (2004) Gamma dose rates and distribution of natural radionuclides in sand beaches – Iiha Grande, Southeastern Brazil.Journal of Environment Radioactivity **75 (2)**: 211 – 223.

Idman, H. (1984) An assessment for phosphates in the carbonatitic alkaline-silicate complexes in Western Kenya, Interim technical report No. 5168, In Industrial mineral project, University of Uppsala, Sweden.

Karam, P. A. (2002) The high background radiation area in Ramsar Iran: Geology, Norm, Biology, LNT, and possible regulatory fun. Proceedings of WM'02 Conference, Feb. 24-28, 2002, Tucson,Arizona.

Kauffman, J. M. (2003) Radiation hormesis. Journal of Scientific Exploration, **17 (3)**: 389-407.

Knoll, G. F. (1997) Radiation Detection and Measurement, John Wiley&Sons, New York.

Lavi, M. M. (1984) A practical approach to quantitative analysis in X-ray fluorescence analysis, M.Sc. thesis, University of Nairobi.

Mangala, J. M. (1987) A multi-channel X-ray fluorescence analyses of fluorspar ore and rock from Mrima hill, Kenya. M.Sc. thesis, Unversity of Nairobi.

McCall, G. J. H. (1958) Geology of the Gwasi area, Ministry of Commerce and Industry, Geology survey of Kenya, Dept. No. 45.

Merdanoglu, B. and Altinsoy, N. (2006) Radioactivity concentrations and dose assessment for soil samples from Kestanbol granite area, Turkey. Rad. Prot. Dosimetry **121(4)**: 399-405.

Mohammadi, S., Taghavi-Dehaghani, M., Mohammad, R.G., Masooni, R., Ghiassi-Nejad, M. (2006) Adaptive response of blood lymphocytes of inhabitants residing in high background radiation areas of Ramsar- Micronuclei, Apoptosis and Comet Assays, J. Radiat. Res., 47, 279-285.

Mohanty, A. K., Sengupta, D., Das, S. K., Vijayan, V ., Saha, S. K. (2004) Natural radioactivity in the new discovered high background radiation area on the eastern coast of Orissa, India, Radiation Measurements. International Congress Series 1276 (38): 153-165.

Morishima, H., Koga, T., Tatsumi, K., Sugahara, T., Wei, L. (2000) Dose measurement, its distribution and individual external dose assessment of inhabitants in the high background radiation areas in China. J. Radiat. Res., 41: 9-23.

Muriithi, A.K. (1982) Multi-element analysis of solid and liquid samples by X-ray fluorescence analysis, M.Sc. thesis, University of Nairobi.

Mustapha, A. O. (1999) Assessment of human exposures to natural sources of radiation in Kenya, Ph.D thesis, University of Nairobi.

Mustapha, A. O., Patel, J. P., Rathore, I. V. S. (1999) Assessment of human exposures to natural sources of radiation. Radiat. Prot. Dosimetry 82 (4): 285-292.

Mustapha, A. O., Patel, J. P., Rathore, I. V. S. (2002) Preliminary report on radon concentration in drinking water and indoor air in Kenya. Environmental Geochemistry and Health 24 (4): 387-396.

NCRP Report, (1987) Ionizing Radiation Exposure of the Population of the United States, National Council for Radiation Protection Report No. 93.

Orris, G. J. and Grauch, R. I. (2002) Raw Earth element mines, Deposits and occurrences, Open-file report 02-189.

Patel, J. P. (1991) Environmental radiation survey of the area of high natural radioactivity of Mrima hill of Kenya, Discovery and Innovation **3(3):** 31-36.

Philips, (1981) The periodic Table of the elements, Netherlands, Almelo.

Rasolonjatovo, A. H., Suzuki, H., Hirabayashi, N., Nunomiya, T., Nakamura, T., Nakao, N., (2002) Measurement for dose-rates of the cosmic-ray components on the ground, J. Radiat. Res., 43: suppl., S27-S33.

Selvasekarapandian, S., Mannikandan, M.N., Sivakumar, R., Balasubramanian, S. (1999) Gamma radiation dose from radionuclides in soil samples of Udagamandalam (Ooty) in India. Radiat. Prot. Dosimetry **82 (3):** 225-228.

Sohrabi, M. (1995) Recent radiological studies of high level natural radiation areas of Ramsar, Iran, International Conference of high levels of natural radiation, Ramsar, 3-7 Nov:, 1990 IAEA, Vienna,71-86.

Sunta, C. M. (1993) A review of the studies of high background areas of the S-W coast of India-Ramsar 3-7, Nov. 1990, IAEA, Vienna, 71-86.

Tahir, S. N. A., Jamil, K., Zaidi, J. H., Arif, M., Ahmed, N., Ahmad, S. A. (2005) Measurement of activity concentrations of naturally occurring radionuclides in soil samples from Punjab province of Pakistan and assessment of radiological hazards. Radiat. Prot. Dosimetry **113 (4):** 421-427.

Tiwari, M. K., Singh, A. K. and Sawhney K. J. S. (2001) Analysis of stainless steel samples by energy-dispersive x-ray fluorescence (EDXRF) spectrometry, Bull. Mater. Sci. **24 (6):** 633-638.

UNSCEAR (1993) Sources of ionizing radiation. United Nations Scientific Committee on the Effects of Atomic Radiation Report to the National Assembly.

UNSCEAR (2000) Sources of ionizing radiation. United Nations Scientific Committee on the Effects of Atomic Radiation Report to the National Assembly.

Wei, L., Zha, Y., Tao, Z., Hew, Chend and Yuan (1993) Epidemiological investigation in high background radiation areas of Yangjiang, China, Ramsar 3-7, International Conference, Nov., 1990, IAEA, Vienna, 523-547.

Wei, L. (1980) Health surveys in high background radiation areas in China, Journal of Science 209(4459): 877-880.